

Recent quantum runtime (dis)advantages

J. Tuziernski,^{1,2} J. Pawłowski,^{3,2} P. Tarasiuk,² L. Pawela,^{4,2} and B. Gardas⁴

¹*Institute of Informatics, National Quantum Information Centre,*

Faculty of Mathematics, Physics and Informatics,

University of Gdańsk, Wita Stwosza 57, 80-308 Gdańsk, Poland

²*Quantumz.io Sp. z o.o., Puławska 12/3, 02-566 Warsaw*

³*Institute of Theoretical Physics, Faculty of Fundamental Problems of Technology,*

Wrocław University of Science and Technology, 50-370 Wrocław, Poland

⁴*Institute of Theoretical and Applied Informatics,*

Polish Academy of Sciences, Baltycka 5, 44-100 Gliwice, Poland

A robust definition of quantum runtime is essential for assessing the performance of quantum algorithms and claims of *quantum advantage*. While for most classical hardware the total runtime is well approximated by computation plus a weakly varying constant, on current quantum hardware a clean experimental separation between “pure computation” and “overhead” is often not justified. Consequently, conventional quantum runtime analyses that exclude substantial system-level overheads (e.g., readout, transpilation, thermalization) can lead to biased performance assessments. In this work we introduce experimentally grounded, end-to-end definitions of quantum runtime for both digital and analogue quantum computers, together with a methodology for selecting strong classical baselines for quantum-classical runtime comparisons. Within this framework, we evaluate recent claims of *quantum advantage* in annealing- and gate-based algorithms. We examine three representative case studies. First, we revisit quantum annealing for approximate QUBO problems [Phys. Rev. Lett. **134**, 160601 (2025)], which employs a well-motivated time-to- ε metric but effectively uses annealing time as a proxy for runtime. Second, we analyze a restricted implementation of Simon’s problem [Phys. Rev. X **15**, 021082 (2025)], where the favorable scaling in oracle calls is undisputed; however, we show that the estimated wall-clock runtime of the quantum experiment is approximately two orders of magnitude slower than a tuned classical baseline at the tested sizes. Finally, we find that the recently reported runtime advantage of the BF-DCQO hybrid algorithm (arXiv:2505.08663) is not observed under more comprehensive benchmarking. Therefore, on current NISQ hardware, runtime-based quantum advantage has not yet been demonstrated under experimentally grounded performance metrics, and credible claims require careful time accounting, appropriate performance measures, and properly chosen classical reference implementations, as discussed in this work.

I. INTRODUCTION

The main motivation for the development of quantum computers, as noted in pioneering works on the subject [1, 2], is the possibility of efficiently solving problems that are currently intractable for classical computation. Initially a theoretical field, quantum computing has seen rapid technological progress, and major roadmaps now predict error-corrected machines by around 2030 [3–5]. Quantum annealing technology is also advancing [6]. Despite this progress, experimentally demonstrating quantum advantage for both paradigms remains a central challenge, driving ongoing research [7].

Quantum advantage can be defined in various ways, including advantages in computation or metrology [8]. One prominent approach relies on complexity-theoretic arguments that establish more favorable scaling than classical algorithms, as exemplified by Simon’s algorithm [9], which exhibits an exponential separation in query complexity, or Shor’s algorithm [10], based on the presumed hardness of factoring [11]. While generic speedups for NP-hard problems are widely believed to be unlikely, restricted instances may admit improvements [12], motivating studies of heuristic quantum algorithms [13]. Such approaches may provide either complexity-theoretic guarantees for specific problem classes or empirical performance improve-

ments on suitable hardware. Other notions of advantage, such as energy efficiency, have also been discussed [14].

As quantum devices continue to improve, increasing attention has turned toward experimental verification of quantum advantage claims [15]. Early demonstrations based on random circuit sampling [16] were subsequently challenged by classical simulation techniques [17, 18], although more recent results appear to lie beyond the reach of known classical methods [19]. Additional experimental claims include favorable time-to-solution scaling for QUBO optimization on D-Wave annealers [20], query-complexity advantages in restricted implementations of Simon’s problem [21], and reported runtime benefits for hybrid classical-quantum algorithms [22]. These studies reflect the growing technological maturity of quantum hardware and are therefore of considerable interest. At the same time, they raise an important question: *Do quantum performance assessment methodologies currently in use – particularly those based on scaling arguments or proxy metrics – result in robust quantum advantage with actual end-to-end runtime improvements critical for practical adoption?*

Specifically, in Sec. II, we discuss challenges associated with defining total runtime in annealing- and gate-based experiments, and propose consistent and operationally meaningful quantum runtime definitions for both quan-

tum computing paradigms. Using those definitions we revisit two recent results regarding quantum advantage for analogue and digital quantum algorithms.

Firstly we address Ref. [20], which reported favorable scaling of a quantum annealing-based approximate QUBO solver relative to a classical reference algorithm (PT-ICM [23]), and show that, when a rigorous end-to-end runtime definition is employed, the reported advantage is no longer observed.

Next, we analyze the results of Ref. [22], where a digitized counter-diabatic quantum optimization algorithm – a gate-based approach – was reported to achieve a runtime advantage over classical simulated annealing (SA) [24] and CPLEX [25]. We find that also in this case the use of the comprehensive runtime definition does not allow concluding that the considered algorithm provides a runtime advantage.

In Sec. III, we address the reported query-complexity advantage for a restricted implementation of Simon’s problem [21] on noisy gate-based IBM quantum processors. We examine whether reduced oracle-call complexity leads to shorter wall-clock runtimes and find that, while the classical algorithm exhibits exponentially worse scaling in oracle calls, its actual runtime in the regime explored in Ref. [21] remains approximately two orders of magnitude shorter than that of the quantum implementation.

Finally, in Sec. IV, we discuss the importance of selecting appropriate classical reference algorithms when evaluating runtime performance. Focusing on runtime as the primary metric, we outline key criteria for classical baseline selection and revisit the choices made in Ref. [22]. We show that adopting an alternative, well-motivated classical reference is sufficient to remove the reported runtime advantage. This situation parallels recent discussions in Ref. [26], where the use of stronger classical baselines was shown to alter conclusions regarding quantum advantage in discrete approximate optimization problems (cf. Ref. [20]) under operationally meaningful conditions. For completeness, we also evaluate the performance of a D-Wave quantum annealer on the instances studied in Ref. [22] and find that, in this setting, adiabatic quantum computing does not yield a runtime advantage. Instead, these instances prove particularly challenging for the annealer, as the required embedding significantly degrades solution quality.

II. QUANTUM ADVANTAGE IN ALGORITHM RUNTIME

In this section, we address the problem of defining runtime in a manner suitable for quantum computation and investigate how sensitive claims of runtime advantage are to changes in this definition. Our focus is on approximate Quadratic Unconstrained Binary Optimization (QUBO), where we assume that the problem has been mapped to an instance of the Ising model, whose ground state encodes the solution [27]. The Ising model, originating from

statistical physics, describes the energy associated with a configuration of discrete variables (spins) $s \in \{-1, 1\}^N$,

$$H(s) = \sum_{i < j} J_{ij} s_i s_j + \sum_i h_i s_i, \quad (1)$$

where J_{ij} are coupling strengths between spins and h_i are local magnetic fields [28].

In the case of approximate optimization, a standard figure of merit is the *time-to-epsilon*, $\text{TT}\varepsilon$ (sometimes used interchangeably with the *time-to-approximation-ratio*, $\text{TT}\mathcal{R}$ [29]), which quantifies the time required to obtain a solution whose energy lies within an ε fraction of the ground-state energy. This quantity is defined as

$$\text{TT}\varepsilon \doteq t_f \cdot \frac{\log(1 - 0.99)}{\log(1 - p_{E \leq E_0 + \varepsilon | E_0})}, \quad (2)$$

where t_f denotes the time taken to generate a single solution and $p_{E \leq E_0 + \varepsilon | E_0}$ is the probability of obtaining a solution with energy E within an ε optimality gap of the true ground-state energy E_0 , when this value is known, or relative to a reference energy otherwise (e.g., the best energy found by a reference solver). In most practical settings, the probability distribution $p_{E \leq E_0 + \varepsilon | E_0}$ is unknown and must be estimated. This typically involves non-trivial optimization of solver parameters, followed by multiple independent runs using the optimized settings, from which the success probability is inferred. Its functional dependence then determines the expected number of repetitions required to obtain a solution within the desired optimality threshold.

Investigations of $\text{TT}\varepsilon$ for specific classes of optimization problems, as well as studies of its scaling with problem size, are commonly used as comparison tools between different heuristic algorithms, including quantum approaches [20]. However, it follows directly from the above definition that a careful and consistent definition of the runtime t_f is essential for fair and unbiased comparisons.

In most cases, defining and measuring runtime for classical algorithms is relatively straightforward, and a variety of mature profiling tools are available for this purpose [30–32]. In contrast, defining and measuring runtime for quantum algorithms presents two key challenges. The first concerns the operational definition of quantum runtime, namely which stages of the quantum computation pipeline should be included in the total runtime. The second concerns the practical measurement of the durations of these stages in an experimental setting. In the following subsections, we address these issues separately for quantum annealing and gate-based quantum devices.

A. Runtime for annealing quantum devices

Solution of an optimization problem on a quantum annealer consists of several stages. First, the optimization problem must be loaded onto the annealing device. This

involves two steps: embedding, which maps a given instance of the Ising model onto the device topology, and programming, which configures the physical parameters of the device to implement the embedded problem. Subsequently, the quantum annealing protocol is executed. It is important to note that the annealing duration is an input parameter to the protocol and, under standard cloud access, cannot be independently measured by the user [33]. Due to the probabilistic nature of the annealing process, multiple runs are typically required to increase the probability of obtaining a high-quality solution. These runs are executed sequentially and are separated by two additional processes: readout, which retrieves information about the final state of each run, and thermalization, which restores the device to its initial state. Both processes contribute non-negligible time overheads.

The comprehensive total runtime definition of a quantum annealer consists of the sum of all annealing runs together with the associated readout, thermalization, and programming times. This definition is not universally adopted; for example, in Ref. [20], runtime was defined solely in terms of the annealing time, with other contributions excluded. Our goal here is to examine how robust is this choice of runtime definition in the context of $\text{TT}\varepsilon$, and to what extent the scaling is affected when additional stages of the annealing protocol are incorporated.

To this end, we repeated the experiments using the same problem instances as in Refs. [20, 34]. When t_f is identified with the annealing time per sample, we reproduce the results reported in Ref. [20], confirming that the methodology was implemented consistently. We then examine how the scaling of $\text{TT}\varepsilon$ changes when t_f is defined as the total QPU access time, including programming, annealing, readout, and thermalization, as reported by the cloud interface [35]. To further validate these results, we also measure the total cloud-access time, which includes additional access-related overheads.

Under these definitions, the results indicate that the effective runtime remains nearly constant over the range of problem sizes considered. An analysis of the scaling exponent supports this observation, as the uncertainties in the fitted exponents are too large to reliably distinguish them from zero. Examining the individual runtime components reveals that readout constitutes the dominant contribution to the total runtime, on the order of $200\ \mu\text{s}$ per annealing run. By comparison, the annealing time in these experiments varies between $0.5\ \mu\text{s}$ and $27\ \mu\text{s}$, indicating that measurement of the final quantum state requires significantly more time than the quantum evolution used to prepare it. This disparity complicates the investigation of $\text{TT}\varepsilon$ scaling and provides context for the exclusion of readout time in Ref. [20]. However, measurement is an intrinsic component of quantum computation – both analog and digital – and the information encoded in a quantum state must ultimately be extracted through readout in order to obtain a solution to the computational problem.

For comparison, we evaluate the scaling behavior of the quantum annealing protocol against a classical Simulated

Bifurcation Machine (SBM [26, 36, 37]); see App. A1. As a classical algorithm, SBM allows direct measurement and decomposition of runtime into components, including the pure computation time, performed on a GPU (t_f^{GPU}), and overhead time (t_f^{overhead}), dominated by data transfer between CPU and GPU and hyperparameter tuning, as described in App. A1. We denote the total runtime from an end-user perspective as $t_f^{\text{tot}} = t_f^{\text{GPU}} + t_f^{\text{overhead}}$. As shown in Fig. 1, the impact of overhead on the scaling of $[\text{TT}\varepsilon]_{\text{Med}}$ is non-negligible, though substantially less pronounced than in the quantum annealing case.

These results indicate that the approximation runtime \approx “compute” + “weakly varying constant” does not hold for current quantum annealers, whereas it remains a reasonable approximation for classical hardware such as GPUs. This difference helps explain why scaling behavior for classical algorithms is typically more robust with respect to the choice of runtime definition.

To fully address this issue, all stages of the quantum computation pipeline would need to be included in the runtime definition. On the corresponding time scales, however, the total runtime becomes nearly constant for the problem sizes accessible in current experiments. Obtaining conclusive scaling results for present-day annealing devices would therefore require experiments with annealing times exceeding $200\ \mu\text{s}$ and substantially larger numbers of qubits.

Our results also allow us to identify another possible route toward a scaling quantum annealing advantage. This concerns a hypothetical scenario in which annealing technology progresses such that the number of qubits increases, while other relevant timescales – in particular the annealing and readout times – remain constant or grow only slowly. Under this assumption, and assuming no comparable improvements in the classical reference technology, a rough extrapolation of the data presented in Fig. 1 suggests that a crossover between the SBM and annealing performance could occur for problem sizes on the order of 10^5 variables.

B. Runtime for digital quantum devices

For digital quantum computers, one can identify computation stages analogous to those discussed for quantum annealers. The initial stage involves preprocessing, in which a quantum circuit is translated into the topology and native gate set of a given device through transpilation. The transpiled circuit is then executed multiple times (shots), with consecutive runs separated by readout and thermalization steps. A comprehensive definition of runtime for digital quantum devices should therefore include all of these processes. This perspective is also adopted in Ref. [38], which outlines procedures for measuring these contributions on IBM quantum devices.

Using this definition of runtime, we revisit the results of Ref. [22]. In that work, a digitized counter-diabatic quantum optimization algorithm was reported to achieve a run-

time advantage over Simulated Annealing (SA [24]) and IBM's proprietary CPLEX solver [25] for a class of Higher-Order Unconstrained Binary Optimization (HUBO) problems. These problems involve cost functions with multi-variable terms of order $N = 3$, generalizing the Ising model in Eq. (1),

$$P(s) = \sum_{\substack{i_1, \dots, i_N \\ i_1 + \dots + i_N \leq 3}} J_{i_1 \dots i_N} s_1^{i_1} \dots s_N^{i_N}. \quad (3)$$

The choice of classical reference algorithms is discussed in Sec. IV. Here, we focus specifically on the definition and measurement of runtime. The algorithm in Ref. [22] is a hybrid quantum-classical procedure consisting of two runs of SA and a single execution of the quantum routine. The first SA run provides an initial guess for the quantum step, and the output of the quantum routine is subsequently refined using a second SA run to mitigate potential readout errors.

The total runtime therefore includes both classical and quantum components. In Ref. [22], the classical runtime was estimated based on the time required to perform a single pass of SA, rather than being directly measured. In addition, overhead contributions associated with SA were not included, although these overheads are reported by the authors to be on the order of 1.6 s. Including such contributions would affect the resulting runtime comparison. Similarly, the quantum runtime was estimated assuming a device throughput of 10^4 circuit executions per second, without explicitly accounting for programming and transpilation overheads. A comprehensive definition of runtime for digital quantum devices should therefore include all of these processes.

Taken together, these considerations indicate that the reported runtime advantage in Ref. [22] is sensitive to the chosen definition and estimate of runtime. Under operationally grounded runtime metrics and consistent accounting of all relevant stages, a runtime advantage is not observed at the present stage. Even under the original measurement assumptions, comparison against stronger classical reference implementations alters the conclusions, as discussed in Sec. IV. A detailed analysis is provided in App. A3.

C. Runtime for classical-quantum algorithms

Heuristic algorithms typically depend on a set of hyperparameters that must be tuned in order to achieve optimal performance [40]. Such tuning can be computationally demanding [41, 42]. As a result, reported solver runtimes that exclude the cost of hyperparameter optimization are difficult to interpret as evidence of a runtime advantage, unless the chosen hyperparameters can be shown to be problem-independent or the tuning effort is applied uniformly across all instances. In addition, for hybrid quantum-classical approaches, runtime accounting should include the overhead associated with data transfer

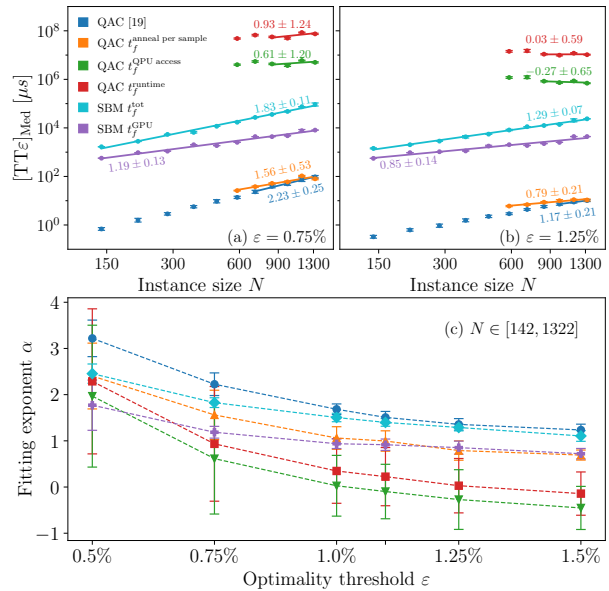


FIG. 1. Time-to-epsilon $[\text{TT}\varepsilon]_{\text{Med}}$ scaling with the size N of the Sidon-28 instances, for values of $\varepsilon = 0.75\%$ in panel (a), and $\varepsilon = 1.25\%$ in panel (b). Results for QAC (blue) solver are reproduced from Ref. [20], courtesy of the authors. Remaining QAC data concerns experiments performed by us on the instances from Ref. [20]. With the same definition of runtime the results (orange) are consistent with [20], which confirms correctness of methodology implementation. In addition $[\text{TT}\varepsilon]_{\text{Med}}$ defined using the complete QPU access time $t_f^{\text{QPU access}}$ as reported by D-Wave's cloud interface (green), as well as runtime measured with cloud access t_f^{runtime} (red) are presented. Solid lines are power-law fits $[\text{TT}\varepsilon]_{\text{Med}} \propto N^\alpha$, with the corresponding exponents α shown on the plot. The instance size range spanned by the lines denote which data points were used for the respective fits. Both plots clearly demonstrate that with the proper runtime definition $[\text{TT}\varepsilon]_{\text{Med}}$ is constant for considered problem sizes. For comparison data for Simulated Bifurcation Machine (SBM) solver [26, 36, 37, 39] with $[\text{TT}\varepsilon]_{\text{Med}}$ computed using 1 GPU and total runtime t_f^{tot} (cyan), as well as pure GPU runtime t_f^{GPU} (magenta) are presented. In this case the scaling of $[\text{TT}\varepsilon]_{\text{Med}}$ is more robust with respect to different runtime definitions, which is generally the case for classical algorithms. The bottom panel (c) shows detailed data of the fitting exponent and its uncertainty for values of $\varepsilon \in \{0.5, 0.75, 1.0, 1.10, 1.25, 1.5\}\%$

between the classical host and the quantum device. This practice is standard in classical heterogeneous computing, such as CPU-GPU workflows, and analogous considerations apply in the quantum-classical context.

Within this framework, we consider the results of Ref. [43], where a quantum-classical solver for large-scale spin-glass problems was proposed and reported to achieve improved solution quality and favorable runtime performance relative to other approaches. The solver operates as a sequential procedure in which each step requires a set of hyperparameters. However, the reported runtimes do not explicitly include the time required to determine these hyperparameters, and the procedure used for their

optimization is not described. Consequently, while the reported solution quality is notable, the available data do not allow for a fully reproducible assessment of end-to-end runtime performance.

From a benchmarking perspective, a more informative comparison would again rely on the time-to-epsilon metric $TT\epsilon$, with all relevant time contributions—including hyperparameter optimization—consistently accounted for, as advocated in Ref. [40].

III. SUPREMACY IN THE ORACLE QUERY COMPLEXITY FRAMEWORK

Oracle query complexity is a well-established framework for analyzing the computational resources required to solve certain classes of problems [44, 45]. The central assumption of this framework is that the problem specification is not fully known; instead, partial information can be obtained by querying an external computational routine, known as an oracle. For example, consider the task of minimizing a function $f(x)$ whose explicit form is unknown to the solution algorithm. The algorithm can interact with the oracle to obtain a function value at a specific point x . The query complexity of the algorithm is then characterized by the number of oracle calls it makes as a function of the problem size.

In general, the query complexity framework applies only to certain families of algorithms that access functions in a way that can be modeled as querying an oracle. It is worth noting that the first theoretical demonstrations of quantum speedup were obtained within this framework [9, 46, 47]. However, once the restriction on limited problem knowledge is lifted, for instance, if the details of an oracle's implementation are made publicly available, the validity of query complexity results no longer holds. In such cases, it becomes possible to design more efficient algorithms that exploit the additional information about the problem specification. See, e.g., the recent discussion in [48] regarding Grover's algorithm.

Here, we aim to interpret the query complexity framework from the perspective of a resource theory. To regard the number of oracle calls as a computational resource, one must assume that the oracle performs the most resource-intensive part of the computation. Only under this assumption can the claim that an algorithm requiring fewer oracle queries is more efficient be justified. Furthermore, even when a separation between the query complexities of different algorithms is proven, it is important to examine how this separation translates into runtime performance. This is particularly relevant in comparing quantum and classical computing, where the operations are characterized by different timescales—typically, a single quantum operation is slower than a classical one [49]. Because of these considerations, it has been argued that a practical quantum advantage can be achieved only by algorithms offering super-quadratic speedups [49]. Runtime analysis thus plays a crucial role in determining the problem scales

at which an oracle query complexity advantage leads to a genuine computational advantage in practice.

Recently, it has been experimentally demonstrated that, for certain problem sizes and even in the presence of uncorrected noise, quantum computers can exhibit an exponential advantage in a variant of Simon's problem [21]. In the original problem, the task is to find a hidden period (a bitstring) encoded in an unknown 2-to-1 function. In contrast, the authors of [21] study N -bit periods with a restricted Hamming weight w (i.e., the number of nonzero bits). In their formulation, the algorithm's figure of merit is defined in terms of a score function, whose primary purpose is to penalize random period-guessing strategies. The authors study scaling of this figure of merit, as a function of the total number of possible periods denoted as $N_w \equiv \sum_j \binom{N}{j}$, where N is the total number of bits, and w the maximal allowed Hamming weight. Theoretical considerations are presented that suggest the possibility of a quantum advantage for such defined problem even for noisy, uncorrected quantum computers. The exponential advantage manifest itself in a polylogarithmic scaling of the score function as a function of the total number of possible periods (the classical model scales polynomially with this parameter). The authors then verify these claims experimentally. An exponential speedup is observed for functions with 29-bit inputs and restricted Hamming weights in the range $w \in [2, 7]$. For larger problem sizes, however, the advantage is destroyed by noise. This raises the question: *how does this favorable scaling relate to the actual runtime of the algorithm?*

To compare the runtimes of quantum and classical algorithms for Simon's problem, we implemented a classical brute-force algorithm running on a single GPU. In Ref. [20], the notion of a *compiler* was introduced to construct an oracle feasible for NISQ devices. The compiler's role is to split the computations performed by Simon's oracle into classical and quantum parts. Its objective is to generate the shallowest possible oracle circuit that can be embedded into the topology of a given NISQ device. A detailed discussion of this compiler can be found in Ref. [20]. For a fair comparison, we implemented a classical oracle corresponding to the quantum oracle described in Ref. [20], and we included only the oracle operation in the runtime. Other computations performed by the compiler were excluded. We assume that any additional classical computations required for the oracle would take the same runtime in both the classical and quantum cases. Furthermore, the comparison does not account for the time needed to construct a shallow quantum circuit. Therefore, in principle, it should also apply to the next generation of quantum devices that will support deeper quantum circuits.

The quantum oracle computes the following classical n -bit function $f_b : \{0, 1\}^n \mapsto \{0, 1\}^n$,

$$f_b(x) = (x_0, \dots, 0, x_{n-i+1} \oplus x_{n-i}, \dots, x_{n-i}), \quad (4)$$

where $b = 0^{n-i} 1^i$ is the function period of Hamming weight i [20]. The additional steps transforming this

function into a generic 2-to-1 function are performed by the classical compiler [21]. In our implementation we relied on the same function form.

The quantum algorithm for Simon's problem was implemented following the approach of Ref. [21], with its runtime estimated using Qiskit functionalities [50]. For each problem size, the quantum circuit was generated and transpiled with the Qiskit compiler (optimization level 3) to account for the connectivity and native gate set of IBM Brisbane [51]. The number of shots was chosen according to the oracle call bound given in Eq. (16) of Ref. [21]. The results are summarized in Fig. 2. The runtime analysis clearly demonstrates that the exponential query complexity speedup reported in [21] does not translate into a faster solution time. For instance, with a problem size of $N = 29$ bits and Hamming weight $w = 7$, the classical brute-force algorithm requires approximately 0.035s to find the solution, while the estimated runtime for the quantum algorithm is on the order of 2s, assuming $s = 10^5$ shots as in the experimental demonstration of Ref. [21]. The projected problem size at which the quantum algorithm would achieve a runtime advantage is $N = 60$. However, as already discussed in Ref. [21], for such problem sizes the impact of noise is too severe to obtain a correct solution to Simon's problem with the quantum algorithm. Let us also stress that the classical algorithm was run on a single general purpose GPU unit. Implementation of this algorithm on a specifically tailored hardware, such as FPGA, would result in even larger separation between classical and quantum runtimes [52].

We emphasize once again that results derived from complexity theory, and query complexity in particular, are typically understood in an asymptotic sense. In contrast, currently available quantum devices restrict us to very small problem sizes. Combined with the fact that quantum and classical computers operate on different timescales for their basic operations, this leads to an important conclusion: a query complexity separation in favor of a quantum algorithm does not necessarily imply a runtime advantage. For certain ranges of problem sizes, algorithms with worse asymptotic scaling may in practice run much faster than those requiring, even exponentially, fewer operations or oracle calls. Similarly, the fastest known algorithm for matrix–matrix multiplication, which scales as $O(n^{2.371339})$ [53], does not provide any practical advantage over optimized implementations of the standard method with $O(n^3)$ scaling.

IV. APPROPRIATE CHOICE OF A CLASSICAL REFERENCE ALGORITHM

A promising approach to identifying quantum advantage for restricted classes of NP-hard instances, where no complexity-theoretic guarantees can be made is the investigation of quantum heuristic methods. In such cases, demonstrating quantum advantage necessarily requires a direct comparison with classical algorithms solving the

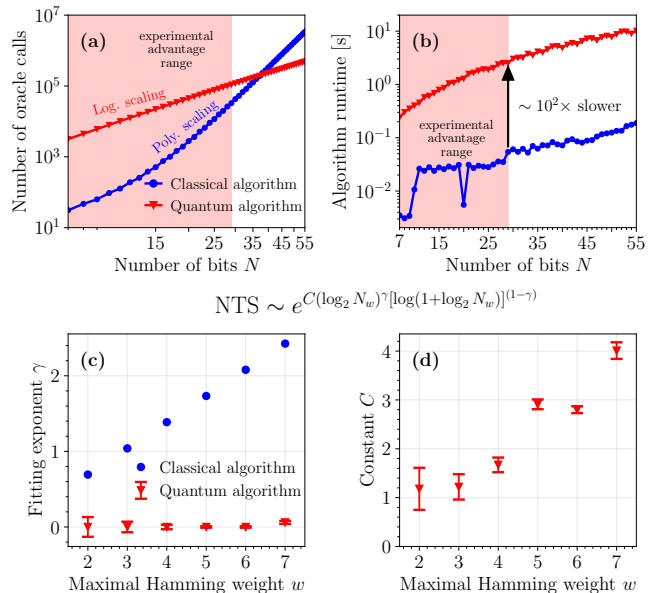


FIG. 2. For the restricted Simon's problem the quantum advantage manifests itself in a favorable polylogarithmic scaling of the protocol score function with the total number of periods $N_w = \sum_j \binom{N}{j}$ as compared to the exponential scaling for the classical algorithm. The score function depends on number of oracle queries and a probability of protocol success. (a) Total number of oracle queries for the protocol and (b) runtime as a function of total number of bits N , as obtained via execution of classical and quantum algorithm solving restricted Simon's problem with $w = 7$. The shaded area indicates sizes of problems, for which the advantage was verified experimentally in [21]. For the considered problem sizes and oracle periods the classical algorithm runtime is shorter than the quantum one, we predict that the runtime crossover occurs for problem sizes $N = 60$. For example, in the case of $N = 29$ bits, what corresponds to the implementation presented in Ref. [21], the runtime of the classical algorithm is two orders of magnitude shorter than the quantum algorithm. The quantum implementation is based on oracle constructed in Ref. [21], and the number of shots required for the algorithm was established using Eq. (16) of Ref. [21]. In this case the quantum circuit was transpiled to take into account connectivity and native gate set of IBM Brisbane, and runtime was estimated using Qiskit functionalities. The classical algorithm was implemented on a GPU. The fitting parameters of the score function for quantum and classical algorithm are presented in panels (c), (d). Parameter $\gamma = 0$ indicates that the score scales polylogarithmically, which implies quantum scaling advantage. The data for the quantum algorithm correspond to the results obtained for IBM Brisbane with dynamical decoupling - Table XX in [21].

same problems. Because classical algorithms are continuously improving in both design and performance, most announcements of quantum supremacy should be understood as claims relative to the state-of-the-art classical methods (see also the related discussion in [12]). This was, for example, the case with the first random circuit sampling-based supremacy results [16–18]. Even though some of these quantum supremacy claims may later be invalidated, they nonetheless represent important mile-

stones on the path toward establishing an unambiguous quantum advantage. At the same time, the choice of the classical reference algorithm must be made with great care, to avoid situations in which the observed quantum speedup arises merely from comparing against a suboptimal classical baseline. This naturally raises the question: *How should the reference algorithm be chosen?*

For heuristic algorithms, there is no universal guideline for selecting the classical reference, and the decision must be made on a case-by-case basis. Nevertheless, several criteria can reasonably guide this choice. First, the selection depends on the quality metric, such as runtime or energy consumption, as well as on the specific problem under consideration. In the context of optimization problems, which form the main focus of this work, arguably the most relevant practical quantity is $\text{TT}\varepsilon$, which measures the expected time required to obtain an approximate solution within a given precision, cf. Eq. 2.

For this figure of merit, an optimal reference classical algorithm should ideally combine solution quality with short runtime. Thus, the most reasonable choices are parallelizable algorithms, whose execution times are significantly shorter than those of sequential approaches, thanks to their ability to fully exploit modern computing resources such as GPUs [54] or FPGAs [55]. In this regard, a particularly interesting class of classical heuristics is based on the dynamics of Hamiltonian nonlinear systems [26, 36, 37, 39, 56–58], as these methods combine good performance with short execution times. Recently, it was shown that one algorithm from this class—the Simulated Bifurcation Machine (SBM)—achieves scaling of $\text{TT}\varepsilon$ comparable to, or better than, that of quantum annealing [26]. This result effectively closes the previously reported quantum-classical gap in approximate optimization announced in [20], where the chosen classical reference was Parallel Tempering with Isoenergetic Cluster Moves (PT-ICM). The PT-ICM algorithm belongs to the class of physics-inspired methods based on temperature annealing [59]. However, unlike algorithms rooted in nonlinear Hamiltonian dynamics, PT-ICM is not straightforwardly parallelizable, and consequently exhibits longer execution times. This makes it a suboptimal reference for comparison with quantum annealing, a conclusion supported by the detailed analysis in [26]. Note that a detailed discussion of the performance of a class of metaheuristic classical algorithms for approximate optimization on cubic-lattice tile-planting models is presented in [60].

Secondly, a classical reference algorithm should be designed to solve the same class of problems. Otherwise, the comparison is biased as it favours the quantum algorithm. The potentially worse performance of a chosen classical algorithm is not evidence of a quantum algorithm advantage but it merely reflects the fact that the problem cannot be solved natively by the classical reference. For example, in [22], the investigated counter-diabatic quantum optimization algorithm is designed to solve HUBO problems, whereas the reference CPLEX solver requires reformula-

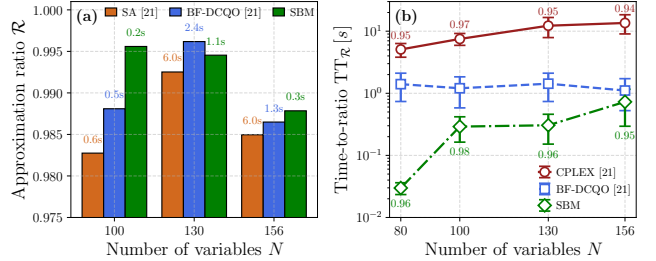


FIG. 3. Partial reproduction of Fig. 5 from Ref. [22], with additional results from SBM solver. Panel (a) shows approximation ratio \mathcal{R} achieved in a time annotated on top of the bars, for instance of type $S_{2q} = 1$, $S_{3q} = 4$ and couplings from Cauchy distribution. The SA and BF-DCQO results from Ref. [22] correspond to a single, best performing instance. Since the exact instances used by the authors of Ref. [22] had not been disclosed, we generated our own instances and show SBM results for the best performing instance. This highlights the risk of selection bias, and the potential for spurious supremacy claims. Finally, panel (b) shows the value of time-to-ratio $\text{TT}\mathcal{R}$ for instances of type $S_{2q} = 1$, $S_{3q} = 6$ and couplings from a symmetrized Pareto distribution, while the annotations indicate the target ratio \mathcal{R} . The results for CPLEX and BF-DCQO are again taken from Ref. [22], where they were obtained as a result of averaging over 5 random instances. Similarly, we constructed our own instances and show SBM results averaged over 5 of them. In both cases SBM outperforms other solvers, casting doubt on the supremacy claim of Ref. [22]. Moreover, in App. A3 we present a more thorough analysis of these instances, and show how to optimize HUBO SA to outperform BF-DCQO.

tion into a mixed-integer program. As the authors note, this reformulation is responsible for the longer runtime of CPLEX compared to their quantum algorithm. Setting aside the fact that the overheads of counter-diabatic quantum optimization were not accounted for (see the discussion in Sec. II), the relevant question is *how the performance of the counter-diabatic quantum optimization algorithm would compare against a classical solver capable of solving HUBO with significantly lower overhead?*

To address this issue, we consider the same class of HUBO problems as in Ref. [22], described by the Hamiltonian of the form

$$H = \sum_{(m,n) \in G_2} J_{mn} \sigma_m^z \sigma_n^z + \sum_{(p,q,r) \in G_3} K_{pqr} \sigma_p^z \sigma_q^z \sigma_r^z, \quad (5)$$

where G_2 and G_3 are the sets of two- and three-body couplings, respectively, and J_{mn} and K_{pqr} are the corresponding coupling strengths. The topology of considered instances is constructed iteratively, starting from the coupling graph C_0 of heavy-hexagonal lattice of IBM's Heron architecture. Each step starts by using graph coloring to identify sets of independent two- and three-body interactions, then S_{2q} (S_{3q}) of them gets included in the G_2 (G_3) set, and finally the coupling graph is modified by performing SWAP operation on pairs of qubits as defined by one of the two-body interactions sets. This procedure creates rather challenging instances, which are

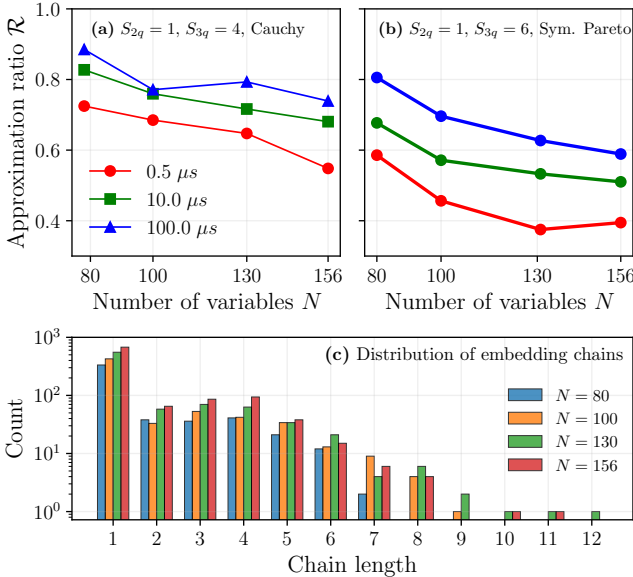


FIG. 4. (a)-(b) Approximation ratio \mathcal{R} achieved by D-Wave’s Advantage2 1.6 quantum annealer on the same HUBO instances as in Fig. 3, computed for each instance type and size, by selecting the best result out of 5 shots with 2^{10} samples each. Forward annealing scheme was used, with annealing times of $0.5\ \mu s$ (red), $10\ \mu s$ (green) and $100\ \mu s$ (blue). The instances were first reduced to QUBO form in the same way as in the case of SBM results (see App. A3 for details), and then embedded into Advantage2 1.6 working graph. The results are, unsurprisingly, much worse than all other considered solvers. They can be explained by investigating the distribution of chain lengths in the necessary embedding, shown in panel (c). Since very long chains are needed to fit the problem instances onto the QPU, the performance of the quantum annealer is severely degraded by possible chain breaks. This highlights an issue that is often overlooked, yet crucial in the context of benchmarking solvers with hardware-imposed constraints on problem topology.

however particularly well suited for the BF-DCQO algorithm, since by changing the number of SWAP iterations, one can directly control the depth of the quantum circuit necessary for the quantum part of the algorithm. The authors of Ref. [22] thus restricted their analysis to only one SWAP iteration, which results in shallow circuits that can be executed on an IBM device in a regime, where the results are not dominated by noise. The instances used in Ref. [22] were not made publicly available [61]. Consequently, we generated our own instances, closely following the description in Ref. [22] (cf. App. A3), and we make both these instances and the generation routine available in the accompanying GitHub [62].

To make a connection with the supremacy claims of Ref. [22], we employ the same figure of merit, which is the time-to-ratio $TT_{\mathcal{R}}$ [29], defined as the time required to find a solution with an energy lower than $\mathcal{R}E_{GS}$, where E_{GS} is the ground state energy of the problem instance. While this metric is conceptually similar to $[TT\epsilon]_{Med}$, its execution in Ref. [22] is questionable, since it does

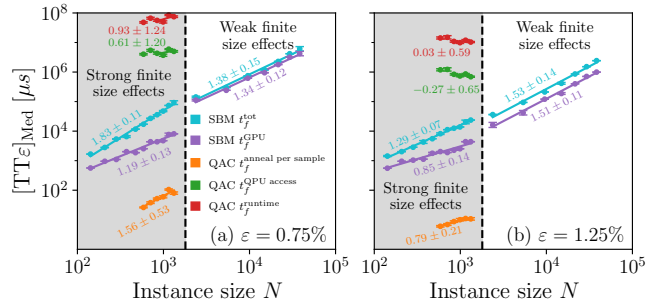


FIG. 5. Illustration of impact of solver-related overhead on scaling behavior of $[TT\epsilon]_{Med}$, as defined in Eq. (2), using a certain type of Ising instances, relevant for near-term quantum devices (see Ref. [26] for details). Note, that the finite size effects diminish significantly beyond the gray-colored region ($N \gtrsim 2000$), as demonstrated with SBM results. However, such system sizes are currently beyond the capabilities of correct quantum annealing devices.

not reflect the stochastic nature of investigated solvers. In Fig. 3, we compare SBM with the results of BF-DCQO, as well as SA and CPLEX taken from Ref. [22]. The authors choose to present their results only for either the best performing instance or as an average over just a few instances. In App. A3, we argue in detail why this approach is not satisfactory, especially for these particular instances, and furthermore, we show that even an optimized version of HUBO-native SA is enough to disprove their supremacy claims. Here, for the sake of the argument, we proceed in a similar fashion, showing SBM data for the best performing instance in Fig. 3(a), and the average over five instances in Fig. 3(b). In both cases, SBM outperforms all other solvers, including BF-DCQO. Nevertheless, we stress that the purpose of this comparison is not to claim any kind of supremacy, but only to highlight how easily such claims can arise from selective reporting.

Nonetheless, an important point is to be made by looking at particular results for $N = 100$ in Fig. 3(a). There, it seems like BF-DCQO retains its advantage, since it achieves a better approximation ratio. However, the difference between SBM and BF-DCQO is minuscule ($\Delta\mathcal{R} \simeq 0.002$), while the corresponding $TT_{\mathcal{R}}$ is smaller by a factor of 2 for SBM. A proper metric for comparing stochastic solvers, such as the time-to-epsilon $[TT\epsilon]_{Med}$ defined in Eq. (2), should take into account both solution quality, and the expected runtime to achieve it.

This analysis illustrates how important it is to select a suitable classical reference algorithm when assessing quantum advantage claims. Let us also mention that the results of [22] were recently also disputed in [63], where it was claimed that the superior performance of BF-DCQO is not due to the quantum routine, as a modified algorithm with the quantum routine replaced by a classical solver exhibits a similar performance. Finally, for the sake of completeness, we tested the performance of D-Wave’s newest quantum annealer, the Advantage2 1.6 based on the Zephyr topology. The results are presented in Fig. 4.

Since the considered instances are not native to the topology of the QPU, an embedding procedure must be carried out. Fig. 4(c) shows the distribution of chain lengths in the embedding, with a tail extending to very long chains. This, unsurprisingly, results in a very poor performance, even after post-selecting the best result out of 35 random instances, and 5 independent shots of 2^{10} samples each. We stress that this is just a single manifestation of a more general issue regarding claims of quantum advantage — the necessity of embedding problem instances onto the hardware graph of a quantum device, often significantly reduces the performance, and thus one should be very careful when making such claims on the basis of experiments with hardware-native problems only.

V. SCALING BEHAVIOR IN SMALL INSTANCES REGIME

Quantum advantage is usually demonstrated by showing that a quantum algorithm exhibits more favorable scaling with respect to the problem size than a reference classical algorithm. Results derived from theoretical considerations, such as those in the oracle query complexity paradigm, are unambiguous. However, when the scaling of heuristic methods is investigated through experiments on quantum hardware, one must account for the fact that, due to the limited number of qubits available in both digital and analog quantum devices, the accessible instance sizes are severely restricted and do not fully meet the requirements for asymptotic scaling. In particular, the scaling behavior of classical algorithms in the problem-size range accessible to current quantum devices—on the order of hundreds of variables for digital hardware and thousands for annealers—may be strongly affected by finite-size effects. Classical algorithms implemented on hardware with timescales comparable to quantum devices, such as GPU clusters or FPGAs, are especially susceptible to overheads that dominate at small scales but become negligible for larger problem sizes. Therefore, despite the limited capabilities of today’s quantum hardware, it is essential to investigate sufficiently large problem sizes in order to establish robust scaling properties. Such a situation was identified in [26] for the SBM, a heuristic inspired by nonlinear Hamiltonian dynamics [36, 37, 39]. The study demonstrated that the scaling properties of this method—specifically its time-to-solution—cannot be reliably inferred when restricted to problem sizes corresponding only to the qubit counts of current quantum annealers. See Fig. 5 for a summary of relevant results.

VI. SUMMARY

Quantum computing has the potential to become a disruptive technology. Realizing this potential, however, requires not only continued technological progress but also the identification of use cases – potentially relevant

for industry – in which quantum methods provide a clear advantage over existing classical approaches. In this work, we adopt a pragmatic perspective in which such an advantage should manifest as a *shorter end-to-end time-to-solution* for a quantum algorithm.

From this perspective, we re-examined several recent claims of quantum advantage and find that, when runtime is defined operationally and compared against appropriately chosen classical references, none of the considered demonstrations establish a practical runtime advantage on current NISQ hardware. We focus in particular on three representative case studies.

Quantum annealing (approximate QUBO). In Ref. [20], runtime was proxied by the annealing time. Using end-to-end runtime measurements, we find that the median $TT\epsilon$ remains approximately constant over the tested problem sizes. This behavior is dominated by the readout time per shot ($\sim 200\ \mu\text{s}$), which exceeds the annealing duration ($0.5\text{--}27\ \mu\text{s}$) by one to two orders of magnitude. As a result, statistical uncertainties are too large to support reliable scaling conclusions over the explored regime (cf. Fig. 1). Moreover, comparison with a stronger classical baseline, such as the Simulated Bifurcation Machine (SBM), indicates that no runtime advantage is observed even under optimistic assumptions regarding the annealing time, consistent with Ref. [26]. SBM exhibits robust scaling behavior at system sizes well beyond those accessible to current quantum annealers (cf. Fig. 5).

Gate-based oracle query (restricted Simon’s problem). While an exponential separation in query complexity is present, wall-clock performance in the experimentally accessible regime favors a tuned classical GPU implementation. For $N = 29$ and restriction parameter $w = 7$ [21], the classical runtime is approximately 0.05 s, whereas the quantum implementation requires roughly 2 s, corresponding to a $\sim 100\times$ difference. Extrapolations suggest a crossover only at $N \approx 60$, which lies beyond the capabilities of current noise-limited devices (cf. Fig. 2).

BF-DCQO hybrid algorithm. Finally, we analyze reported performance gains for solving HUBO instances [22]. We find that these conclusions rely on runtime estimates and limited statistical sampling, which complicate a reproducible assessment of end-to-end performance. In particular, the problem instances considered were designed to align with specific hardware characteristics [64] and require substantially richer statistics to support claims of systematic advantage. Our analysis shows that, under consistent timing protocols and broader sampling, the reported performance differences are not robust (cf. Fig. 3 and App. A3).

In summary, across all examined cases, a practical runtime advantage on current NISQ hardware is not observed under experimentally grounded performance metrics. Credible claims of runtime quantum advantage require careful accounting of dominant overheads (including readout, thermalization, and compilation), the use of well-defined metrics such as $TT\epsilon$ with appropriate optimization, and benchmarking against state-of-the-art classical

solvers selected impartially for the problem class under consideration.

VII. OUTLOOK

No single, universal procedure exists for evaluating quantum advantage, since different problem classes and computational paradigms exhibit distinct characteristics. Nevertheless, a set of general principles can be distilled from our analysis. In the context of runtime-based quantum advantage, we summarize these principles as follows:

- **Primary Runtime Measurement:** Runtime measurements should be obtained from direct timing of executions, rather than inferred from nominal device parameters or documentation.
- **Comprehensive Overhead Accounting:** Runtime should be reported as a direct measurement of the total execution time, including all relevant system-level overheads such as readout, compilation, data transfer, and hyperparameter tuning.
- **Standardized Performance Metrics:** Performance should be evaluated using well-defined and widely accepted metrics, such as the time-to- ε for sufficiently small values of ε , with results assessed across diverse problem instances and structures.
- **Scaling Integrity:** Scaling analyses should span a sufficiently broad range of problem sizes to capture asymptotic behavior, and extrapolations beyond the measured regime should be treated with appropriate caution.
- **High-Performance Classical Baselines:** Classical reference algorithms should be selected with care, taking into account the current state of algorithmic development and implementation-level optimizations.
- **The Hybrid Null Hypothesis:** For hybrid quantum-classical algorithms, a suitable null hy-

pothesis should be tested, namely whether replacing the quantum subroutine with a purely classical counterpart yields comparable or improved performance.

We stress that these principles are intended as general guidance rather than problem-specific prescriptions, and are not meant to constitute an exhaustive set of criteria.

We emphasize that while energy efficiency is a potentially relevant dimension of quantum advantage [14], the present work deliberately focuses on runtime-based performance metrics. At the current level of user access to quantum hardware, energy consumption cannot be independently verified or consistently defined, as it depends on system-level factors such as cryogenics and control electronics that are typically not transparent to the user. At the same time, contemporary high-performance classical accelerators, such as modern GPUs, typically operate at sub-kilowatt power levels, underscoring the importance of clearly defined system boundaries when comparing different computational platforms. The development of verifiable and reproducible energy-efficiency metrics therefore remains an important open challenge for future benchmarking efforts.

As a final note, while the present work does not focus on system-level capability metrics such as Quantum Volume [65] and CLOPS [66], we note that such metrics provide a valuable and complementary means of tracking technological progress in quantum hardware, particularly at the level of device capability and system throughput.

ACKNOWLEDGMENTS

This project was supported by the National Science Center (NCN), Poland, under Projects: Sonata Bis 10, No. 2020/38/E/ST3/00269 (B.G) Quantumz.io Sp. z o.o acknowledges support received from The National Centre for Research and Development (NCBR), Poland, under Project No. POIR.01.01.01-00-0061/22.

[1] R. P. Feynman, Simulating physics with computers, *Int. J. Theor. Phys.* **21**, 467–488 (1982).

[2] D. Deutsch, Quantum theory, the Church-Turing principle and the universal quantum computer, *Proc. R. Soc. Lond. A* **400**, 97 (1985).

[3] IonQ, *IonQ Roadmap* (2025).

[4] IBM, *IBM Quantum Roadmap* (2025).

[5] Quantinuum, *Quantinuum Roadmap* (2025).

[6] D-Wave, *The D-Wave Clarity Roadmap* (2025), accessed: 2025-01-30.

[7] D. Castelvecchi, Quantum computers will finally be useful: what's behind the revolution, *Nature* **650**, 24 (2026).

[8] H.-Y. Huang, S. Choi, J. R. McClean, and J. Preskill, The vast world of quantum advantage, [arXiv:2508.05720](https://arxiv.org/abs/2508.05720) (2025).

[9] D. R. Simon, On the power of quantum computation, *SIAM J. Comput.* **26**, 1474 (1997).

[10] P. Shor, Algorithms for quantum computation: discrete logarithms and factoring, in *Proceedings 35th Annual Symposium on Foundations of Computer Science* (1994) pp. 124–134.

[11] L. J. Stockmeyer, The polynomial-time hierarchy, *Theor. Comput. Sci.* **3**, 1 (1976).

[12] O. Lanes, M. Beji, A. D. Corcoles, C. Dalyac, J. M. Gambetta, L. Henriet, A. Javadi-Abhari, A. Kandala,

A. Mezzacapo, C. Porter, and et al., [A Framework for Quantum Advantage](#) (2025), [arXiv:2506.20658 \[quant-ph\]](#).

[13] A. Abbas, A. Ambainis, B. Augustino, A. Bärtschi, H. Buhrman, C. Coffrin, G. Cortiana, V. Dunjko, D. J. Egger, B. G. Elmegreen, and N. Franco et al., Challenges and opportunities in quantum optimization, [Nat. Rev. Phys. 6 \(2024\)](#).

[14] F. Meier and H. Yamasaki, Energy-consumption advantage of quantum computation, [PRX Energy 4 \(2025\)](#).

[15] K. Bertels, E. Turki, T. Sarac, A. Sarkar, and I. Ashraf, Quantum computing – a new scientific revolution in the making, [arXiv:2106.11840 \(2024\)](#).

[16] F. Arute, K. Arya, R. Babbush, D. Bacon, J. C. Bardin, R. Barends, R. Biswas, S. Boixo, F. G. S. L. Brandao, and D. A. Buell et al., Quantum supremacy using a programmable superconducting processor, [Nature 574, 505 \(2019\)](#).

[17] Y. A. Liu, X. L. Liu, F. N. Li, H. Fu, Y. Yang, J. Song, P. Zhao, Z. Wang, D. Peng, H. Chen, and et al., Closing the "quantum supremacy" gap: achieving real-time simulation of a random quantum circuit using a new Sunway supercomputer, in [Proc. - Int. Conf. High Perform. Comput. Netw. Storage Anal.](#), SC '21 (Association for Computing Machinery, New York, NY, USA, 2021).

[18] F. Pan, K. Chen, and P. Zhang, Solving the sampling problem of the Sycamore quantum circuits, [Phys. Rev. Lett. 129, 090502 \(2022\)](#).

[19] A. Morvan, B. Villalonga, X. Mi, S. Mandrà, A. Bengtsson, P. V. Klimov, Z. Chen, S. Hong, C. Erickson, and I. K. Drozdov et al., Phase transitions in random circuit sampling, [Nature 634, 328 \(2024\)](#).

[20] H. Munoz-Bauza and D. Lidar, Scaling advantage in approximate optimization with quantum annealing, [Phys. Rev. Lett. 134, 160601 \(2025\)](#).

[21] P. Singkanipa, V. Kasatkin, Z. Zhou, G. Quiroz, and D. A. Lidar, Demonstration of algorithmic quantum speedup for an abelian hidden subgroup problem, [Phys. Rev. X 15 \(2025\)](#).

[22] P. Chandarana, A. G. Cadavid, S. V. Romero, A. Simen, E. Solano, and N. N. Hegade, Runtime quantum advantage with digital quantum optimization, [arXiv:2505.08663 \(2025\)](#).

[23] Z. Zhu, A. J. Ochoa, and H. G. Katzgraber, Efficient cluster algorithm for spin glasses in any space dimension, [Phys. Rev. Lett. 115, 077201 \(2015\)](#).

[24] S. Kirkpatrick, C. D. Gelatt, and M. P. Vecchi, Optimization by Simulated Annealing, [Science 220, 671 \(1983\)](#).

[25] CPLEX, IBM ILOG, [Users manual for CPLEX](#) (2024).

[26] J. Pawłowski, P. Tarasiuk, J. Tuziński, L. Pawela, and B. Gardas, Closing the quantum-classical scaling gap in approximate optimization, [arXiv:2505.22514 \(2025\)](#).

[27] S. Boettcher, Analysis of the relation between quadratic unconstrained binary optimization and the spin-glass ground-state problem, [Phys. Rev. Res. 1, 033142 \(2019\)](#).

[28] G. F. Newell and E. W. Montroll, On the Theory of the Ising Model of Ferromagnetism, [Rev. Mod. Phys. 25, 353 \(1953\)](#).

[29] M. Mohseni, M. M. Rams, S. V. Isakov, D. Eppens, S. Pielawa, J. Strumpfer, S. Boixo, and H. Neven, Sampling diverse near-optimal solutions via algorithmic quantum annealing, [Phys. Rev. E 108 \(2023\)](#).

[30] NVIDIA, [Nsight systems user guide](#) (2025).

[31] Intel, [Intel vtune profiler](#) (2025).

[32] AMD, [AMD profiler](#) (2025).

[33] D-Wave, [D-wave QPU solver parameters](#) (2025).

[34] H. Munoz Bauza and D. Lidar, [Scaling Advantage in Approximate Optimization with Quantum Annealing - Spin-Glass Instances](#) (2025).

[35] D-Wave, [D-wave operation and timing](#) (2025).

[36] H. Goto, Bifurcation-based adiabatic quantum computation with a nonlinear oscillator network, [Sci. Rep. 6, 21686 \(2016\)](#).

[37] H. Goto, K. Endo, M. Suzuki, Y. Sakai, and Taro et al., High-performance combinatorial optimization based on classical mechanics, [Sci. Adv. 7, eabe7953 \(2021\)](#).

[38] T. Koch, D. E. B. Neira, Y. Chen, G. Cortiana, D. J. Egger, R. Heese, N. N. Hegade, A. G. Cadavid, and et al., Quantum optimization benchmark library – the intractable decathlon, [arXiv:2504.03832 \(2025\)](#).

[39] H. Goto, K. Tatsumura, and A. R. Dixon, Combinatorial optimization by simulating adiabatic bifurcations in nonlinear hamiltonian systems, [Sci. Adv. 5, eaav2372 \(2019\)](#).

[40] T. F. Rønnow, Z. Wang, J. Job, S. Boixo, S. V. Isakov, D. Wecker, J. M. Martinis, D. A. Lidar, and M. Troyer, Defining and detecting quantum speedup, [Science 345, 420–424 \(2014\)](#).

[41] E. Alessandroni, S. Ramos-Calderer, I. Roth, E. Traversi, and L. Aolita, Alleviating the quantum big-m problem, [npj Quantum Inf. 11 \(2025\)](#).

[42] M. Larocca, S. Thanasilp, S. Wang, K. Sharma, J. Biamonte, P. J. Coles, L. Cincio, J. R. McClean, Z. Holmes, and M. Cerezo, Barren plateaus in variational quantum computing, [Nat. Rev. Phys. 7, 174–189 \(2025\)](#).

[43] S. Schulz, D. Willsch, and K. Michielsen, Learning-driven annealing with adaptive hamiltonian modification for solving large-scale problems on quantum devices, [arXiv:2502.21246 \(2025\)](#).

[44] R. Kothari, T. Lee, M. Szegedy, and I. Newman, [Query Complexity](#), G - Reference, Information and Interdisciplinary Subjects Series (World Scientific Publishing Company Pte Limited, 2025).

[45] A. Ambainis, Understanding quantum algorithms via query complexity, [arXiv:1712.06349 \(2017\)](#).

[46] D. Deutsch and R. Jozsa, Rapid solution of problems by quantum computation, [Proc. R. Soc. A 439, 553 \(1992\)](#).

[47] L. K. Grover, A fast quantum mechanical algorithm for database search, in [Proc. Annu. ACM Symp. Theory Comput.](#) (1996) pp. 212–219.

[48] E. M. Stoudenmire and X. Waintal, Opening the black box inside grover's algorithm, [Phys. Rev. X 14, 041029 \(2024\)](#).

[49] T. Hoefler, T. Häner, and M. Troyer, Disentangling hype from practicality: On realistically achieving quantum advantage, [Commun. ACM 66, 82 \(2023\)](#).

[50] A. Javadi-Abhari, M. Treinish, K. Krsulich, C. J. Wood, J. Lishman, J. Gacon, S. Martiel, P. D. Nation, L. S. Bishop, A. W. Cross, B. R. Johnson, and J. M. Gambetta, Quantum computing with qiskit, [arXiv:2405.08810 \(2024\)](#).

[51] IBM, [IBM Quantum compute resources](#) (2025).

[52] S. Chowdhury, N. A. Aadit, A. Grimaldi, E. Raimondo, A. Raut, P. A. Lott, J. H. Mentink, M. M. Rams, F. Ricci-Tersenghi, M. Chiappini, L. S. Theogarajan, T. Srimani, G. Finocchio, M. Mohseni, and K. Y. Camsari, Pushing the boundary of quantum advantage in hard combinatorial optimization with probabilistic computers, [arXiv:2503.10302 \(2025\)](#).

[53] J. Alman, R. Duan, V. V. Williams, Y. Xu, Z. Xu, and R. Zhou, More asymmetry yields faster matrix multiplication, [arXiv:2404.16349](https://arxiv.org/abs/2404.16349) (2024).

[54] X. Yi, A Study of Performance Programming of CPU, GPU accelerated Computers and SIMD Architecture, [arXiv:2409.10661](https://arxiv.org/abs/2409.10661) (2024).

[55] R. Kastner, J. Matai, and S. Neuendorffer, Parallel Programming for FPGAs, [arXiv:1805.03648](https://arxiv.org/abs/1805.03648) (2018).

[56] J. Hou, A. Barzegar, and H. G. Katzgraber, Direct comparison of stochastic driven nonlinear dynamical systems for combinatorial optimization, *Phys. Rev. E* **112**, 035301 (2025).

[57] T. Aonishi, T. Nagasawa, T. Koizumi, M. D. S. H. Guanathilaka, K. Mimura, M. Okada, S. Kako, and Y. Yamamoto, Highly Versatile FPGA-Implemented Cyber Coherent Ising Machine, *IEEE Access* **12**, 175843–175865 (2024).

[58] J. Pawłowski, J. Tuziemski, P. Tarasiuk, A. Przybysz, R. Adamski, K. Hendzel, L. Pawela, and B. Gardas, VeloxQ: A fast and efficient QUBO solver, [arXiv:2501.19221](https://arxiv.org/abs/2501.19221) (2025).

[59] D. Delahaye, S. Chaimatanan, and M. Mongeau, Simulated annealing: From basics to applications, in *Handbook of Metaheuristics*, edited by M. Gendreau and J.-Y. Potvin (Springer International Publishing, Cham, 2019) pp. 1–35.

[60] A. A. Gangat, Linear-time classical approximate optimization of cubic-lattice classical spin glasses, *Physical Review Applied* **25**, [10.1103/1103.1144-k42k](https://doi.org/10.1103/1103.1144-k42k) (2026).

[61] The authors did not respond to our request to share their HUBO instances.

[62] J. Tuziemski, J. Pawłowski, P. Tarasiuk, L. Pawela, and B. Gardas, Recent quantum runtime (dis)advantages – code repository, <https://github.com/quantumz-io/quanutm-runtime-disadvantage> (2025), GitHub repository.

[63] P. Farré, E. Ordóñez, K. Chern, and C. C. McGeoch, Comparing Quantum Annealing and BF-DCQO, [arXiv:2509.14358](https://arxiv.org/abs/2509.14358) (2025).

[64] IBM, IBM Quantum Platform - Processor types (2025).

[65] A. W. Cross, L. S. Bishop, S. Sheldon, P. D. Nation, and J. M. Gambetta, Validating quantum computers using randomized model circuits, *Phys. Rev. A* **100**, 032328 (2019).

[66] A. Wack, H. Paik, A. Javadi-Abhari, P. Jurcevic, I. Faro, J. M. Gambetta, and J. M. Chow, Quality, speed, and scale: three key attributes to measure the performance of near-term quantum computers, [arXiv:2110.14108](https://arxiv.org/abs/2110.14108) (2021).

[67] T. Zhang and J. Han, Quantized simulated bifurcation for the Ising model, in *2023 IEEE 23rd International Conference on Nanotechnology (NANO)* (2023) pp. 715–720.

[68] J. Fulman, Random matrix theory over finite fields: a survey, [arXiv:0003195](https://arxiv.org/abs/0003195) (2001).

[69] C. Chamberland, G. Zhu, T. J. Yoder, J. B. Hertzberg, and A. W. Cross, Topological and subsystem codes on low-degree graphs with flag qubits, *Phys. Rev. X* **10** (2020).

[70] N. Dattani, Quadratization in discrete optimization and quantum mechanics, [arXiv:1901.04405](https://arxiv.org/abs/1901.04405) (2019).

[71] T. Kanao and H. Goto, Simulated bifurcation for higher-order cost functions, *Appl. Phys. Express.* **16**, 014501 (2022).

[72] D. J. Earl and M. W. Deem, Parallel tempering: Theory, applications, and new perspectives, *Phys. Chem. Chem. Phys.* **7**, 3910 (2005).

[73] A. Russkov, R. Chulkevich, and L. N. Shchur, Algorithm for replica redistribution in an implementation of the population annealing method on a hybrid supercomputer architecture, *Comput. Phys. Commun.* **261**, 107786 (2021).

[74] J. Machta, Population annealing with weighted averages: A monte carlo method for rough free-energy landscapes, *Phys. Rev. E* **82**, 026704 (2010).

[75] S. V. Romero, A.-M. Visuri, A. G. Cadavid, E. Solano, and N. N. Hegade, Bias-field digitized counterdiabatic quantum algorithm for higher-order binary optimization, [arXiv:2409.04477](https://arxiv.org/abs/2409.04477) (2024).

Appendix A1: Simulated Bifurcation Machine

To demonstrate that the results for classical algorithms are less sensitive to runtime definition changes we consider a discretized version of Simulated Bifurcation Machine algorithm [26, 36, 37, 39], first introduced as dSB in Ref. [37]. The algorithm is based on a non-linear Hamiltonian system, whose motion is governed by the following equations:

$$\begin{aligned} \dot{q}_i &= a_0 p_i, \\ \dot{p}_i &= -[a_0 - a(t)] q_i + c_0 \left(\sum_{j=1}^N J_{ij} f(q_j) + h_i \right), \end{aligned} \quad (\text{A11})$$

where $f(x) = \text{sign}(x)$ is the signum function. The original formulation of dSB is modified to include a ternary discretization scheme [67], replacing sign with

$$f(x) = \begin{cases} 0 & |x| \leq \Delta(t), \\ \text{sign}(x) & |x| > \Delta(t), \end{cases} \quad (\text{A12})$$

where $\Delta(t) = 0.7 \frac{t}{T}$ is a time-dependent threshold and T is the total time of the evolution.

The nonlinearity predominantly stems from perfectly inelastic walls that are inserted at $|q_i| = 1$, and after hitting a wall ($|q_i| > 1$), the particle position q_i is set to $\text{sign}(q_i)$ and its momentum to $p_i = 0$. The system's evolution depends on a set of hyperparameters. Hyperparameters a_0 and c_0 are typically set to $a_0 = 1$ and $c_0 = \frac{0.7a_0}{\sigma\sqrt{N}}$, where σ is the standard deviation of off-diagonal matrix elements of J . The system undergoes bifurcations, which are caused by a change of the linear time-dependent function $a(t) = \frac{t}{T}$. Bifurcations change the system's energy landscape to one approximately encoding the local minima of the Ising term. This mechanism allows to find low-energy solutions of the binary optimization problem by binarizing the final system's state, taking $s_i = \text{sign}(q_i)$. The SBM is a stochastic system sensitive to initial conditions, a large number of independent replicas can be integrated simultaneously from different starting points, enabling massive parallelization. The remaining hyperparameters are Δt - time step, and N_s - number of steps, which determine jointly the total evolution time $T = N_s \Delta t$. Since SBM is a stochastic algorithm it needs to be executed a number of times, which we denote as number of replicas N_r (this can be done in parallel). For each replica the timestep δt is chosen randomly, for details see [26].

Appendix A2: Benchmarking classical algorithm on pseudo-random simulated oracles

The Simon's problem for a function that simulates behavior of an oracle can be solved using a classical algorithm. We have used a solver that not only confirms existence of a non-zero period, but also finds the period. The series of tests and benchmarks we have performed require simulation of oracle-like 2-to-1 functions. Given the number of bits n , a function $f : \{0, 1\}^n \mapsto \{0, 1\}^n$ with period $p \in \{0, 1\}^n \setminus \{0\}^n$ needs to match the following property:

$$\forall_{x, y \in \{0, 1\}^n} \quad f(x) = f(y) \iff y = x \oplus p. \quad (\text{A21})$$

Given a 1-to-1 function $g : \{0, 1\}^n \mapsto \{0, 1\}^n$ and ordering \prec over $\{0, 1\}^n$, one can define a function

$$f(x) = g(\min_{\prec}(x, x \oplus p)). \quad (\text{A22})$$

that meets the requirements. The \prec used in our benchmarks was the lexicographic ordering of bit tuples. The other possible orderings can be achieved by comparing $h(x)$ and $h(x \oplus p)$ for 1-to-1 functions $h : \{0, 1\}^n \mapsto \{0, 1\}^n$ instead.

Since we can build the right function for any given period, properties of the period, such as number of set bits, can be assigned arbitrarily. The last step to consider is construction of 1-to-1 functions such as g . To include all f_b functions from (4), we have implemented affine functions over GF(2) field:

$$g(x) = Ax \oplus b \quad \text{for} \quad A \in \{0, 1\}^{n \times n}, \quad \text{rank}_{\text{GF}(2)} A = n, \quad b \in \{0, 1\}^n. \quad (\text{A23})$$

Notably, Ax is also intended to be computed in GF(2). Requirement that $\text{rank}_{\text{GF}(2)} A = n$ is equivalent to A being invertible in GF(2), which is crucial to g being a bijection.

ALG. 1. Simulated Bifurcation Machine.**Input:**

J, h – coupling matrix and local fields vector specifying an instance of the Ising model,
 Δt – time step,
 N_s – number of steps,
 $a(t)$ – pump function,
 $f(x)$ – discretization function,
 a_0, c_0 – hyperparameters.

Output:

E, q – energy and its corresponding state of the found minimum.

$n = \text{length}(h)$

$q_1 \leftarrow \{\text{rand}(-1, 1)\}^n$

$p_1 \leftarrow \{\text{rand}(-1, 1)\}^n$

for $j = 1, \dots, N_s$ **do**

$q_{i+1} \leftarrow a_0 \Delta t p_i$

$p_{i+1} \leftarrow \left\{ [a_0 - a(j \Delta t)] q_i + c_0 \left(\sum_{j=1}^N J_{ij} f(q_j) + h_i \right) \right\} \Delta t$

for $i = 1, \dots, n$ **do**

if $q_{i+1,j} \geq |1|$ **then**

$q_{i+1,j} \leftarrow \text{sign}(q_{i+1,j})$

$p_{i+1,j} \leftarrow 0$

end if

end for

end for

$x = \text{sign}(x_{N_s+1})$

$E = \frac{1}{2} x^T J x + h^T x$

return E, x

Pseudo-random generation of A and b is straightforward to implement. Constraint on A needs to be considered – probability that a pseudo random $\{0, 1\}^{n \times n}$ matrix will be invertible in GF(2) decreases with n . However, as shown in [68], it converges to a constant that exceeds 1/4, which makes it practically viable to generate matrices in a loop until finding a matrix with rank n .

Wider selection of g functions (and order-altering h) can be achieved by applying complex strategies, including cryptographic schemes such as AES with a fixed key unknown to the solver. The proposed choice of skipping h and using affine g is a compromise that ensures the oracle is non-trivial, and includes all cases described in (4).

The classical Alg. 2 is oblivious to the inner implementation of the oracle. The oracle-like function is applied for all the x vectors such that either $(x_1, \dots, x_{\lfloor n/2 \rfloor})$ or $(x_{\lfloor n/2 \rfloor + 1}, \dots, x_n)$ are all zeros. For any period p , both higher $\lceil n/2 \rceil$ and lower $\lfloor n/2 \rfloor$ bits of p will be tested – so there is exactly one pair x_i, x_j such that $f(x_i) = f(x_j)$, yielding $p = x_i \oplus x_j$. The total number of vectors to evaluate is $2^{\lceil n/2 \rceil} + 2^{\lfloor n/2 \rfloor} - 1$. In our scenario, the complexity is in $\Theta(n^2 2^{n/2})$. That cost is reached both by evaluating of the linear functions, and by sorting evaluation results, which involves comparisons of n -bit vectors.

1. Polynomial scaling for restricted Simon's problem with fixed w

The proposed classical algorithm can be further optimized for solving restricted Simon's problem with $w < \lceil n/2 \rceil$. A period p with at most w set bits can always be decomposed into $p = x_i \oplus x_j$ such that x_i and x_j have at most w set bits in total. Retaining the core concept from the general approach, this can be achieved by x_i with $\lceil n/2 \rceil$ lowest bits of p , and x_j with the remaining $\lfloor n/2 \rfloor$ highest bits.

In order to find the decomposition in a single pass, we can constrain both x_i and x_j to have at most w set bits, rather than w bits set in total. This approach remains highly efficient for parallel computations, as demonstrated by the runtime measurements from Fig. 2. Constrained vectors can be generated with Alg. 3. The required precomputation of $S(m, k) = \sum_{v=0}^k \binom{m}{v}$ values involves $\Theta(n^2)$ computational and memory cost, and is calculated once per n , and reusable across multiple solver calls.

ALG. 2. Classical solver to Simon's problem.**Input:**

n – number of bits,
 $f : \{0, 1\}^n \mapsto \{0, 1\}^n$ function that evaluates oracle.

Output:

$p \in \{0, 1\}^n$ – oracle period, zeros when there is none.
 $x_1 \leftarrow \{0\}^n$
for $i = 1, \dots, 2^{\lceil n/2 \rceil} - 1$ **do**
 $x_{i+1} \leftarrow (\lceil n/2 \rceil \text{ lowest bits of } i, 0 \dots)$
end for
for $i = 1, \dots, 2^{\lfloor n/2 \rfloor} - 1$ **do**
 $x_{i+2^{\lceil n/2 \rceil}} \leftarrow (0 \dots, \lfloor n/2 \rfloor \text{ lowest bits of } i)$
end for
for $i = 1, \dots, 2^{\lceil n/2 \rceil} + 2^{\lfloor n/2 \rfloor} - 1$ **do**
 $y_i \leftarrow f(x_i)$
end for
 $(j_1, \dots, j_{2^{\lceil n/2 \rceil} + 2^{\lfloor n/2 \rfloor} - 1}) \leftarrow \text{SortingPermutation}(y_1, \dots, y_{2^{\lceil n/2 \rceil} + 2^{\lfloor n/2 \rfloor} - 1})$ ▷ done by sorting indices with y as key
for $i = 1, \dots, 2^{\lceil n/2 \rceil} + 2^{\lfloor n/2 \rfloor} - 2$ **do**
 if $y_{j_i} = y_{j_{i+1}}$ **then**
 return $x_{j_i} \oplus x_{j_{i+1}}$
 end if
end for
return $\{0\}^n$

The adjusted solver for restricted Simon's problem described in Alg. 4 is a specialized version of Alg. 2 where only vectors x_i with up to w set bits are constructed and used in duplicate search. For small fixed w , specifically $w \leq n/4$, the total number of vectors processed is

$$\begin{aligned}
 v(n, w) &= S(\lfloor n/2 \rfloor, w) + S(\lceil n/2 \rceil, w) \leq \\
 &\leq 2S(\lceil n/2 \rceil, w) \leq 2\lceil n/2 \rceil \binom{\lceil n/2 \rceil}{w} = \\
 &= 2\lceil n/2 \rceil \prod_{i=1}^w \frac{\lceil n/2 \rceil - i + 1}{i} \leq 2\lceil n/2 \rceil^{w+1}.
 \end{aligned} \tag{A24}$$

The most dominant component to Alg. 4 complexity is sorting an array of $v(n, w)$ bit vectors of length n . This operation is $\Theta(v(n, w) \cdot \log(v(n, w)) \cdot n)$. For small or fixed w , the bound from Eq. A24 applies, so the complexity is in the class $O(w n^{w+2} \log n)$. This shows that the proposed classical solver for restricted Simon's problem has a polynomial complexity for fixed w . The polynomial behavior can be observed in Fig. 2.

ALG. 3. Computing the i -th vector within limit of w set bits.**Input:**

n – number of bits,
 $w \leq n$ – maximum number of set bits,
 $i \in \{0, \dots, (\sum_{v=0}^w \binom{n}{v}) - 1\}$ – index of vector.
 $S(m, k) = \sum_{v=0}^k \binom{m}{v}$ – precomputed values for $m = \{0, \dots, n\}$ and $k = \{0, \dots, m\}$.

Output:

$x \in \{0, 1\}^n$ – the i -th vector meeting the constraint in lexicographic order.
 $x \leftarrow \{0\}^n$
 $v \leftarrow w$
for $b = 1, \dots, n$ **do**
 if $i \geq S(n - b, v)$ **then**
 $x_b \leftarrow 1$
 $i \leftarrow i - S(n - b, v)$
 $v \leftarrow v - 1$
 end if
end for
return x

ALG. 4. Classical solver to restricted Simon problem.**Input:**

n – number of bits,
 $f: \{0, 1\}^n \mapsto \{0, 1\}^n$ function that evaluates oracle,
 $w \leq n$ – maximum number of set bits in oracle period,
 $S(m, k) = \sum_{v=0}^k \binom{m}{v}$ – precomputed values for $m = \{0, \dots, n\}$ and $k = \{0, \dots, m\}$.

Output:

$p \in \{0, 1\}^n$ – oracle period, zeros when there is none.
 $x_1 \leftarrow \{0\}^n$
for $i = 1, \dots, S(\lceil n/2 \rceil, \min\{w, \lceil n/2 \rceil\})$ **do**
 $t \leftarrow \text{ALG3}(\lceil n/2 \rceil, \min\{w, \lceil n/2 \rceil\}, i, S)$
 $x_{i+1} \leftarrow (\lceil n/2 \rceil \text{ lowest bits of } t, 0\dots)$
end for
for $i = 1, \dots, S(\lfloor n/2 \rfloor, \min\{w, \lfloor n/2 \rfloor\})$ **do**
 $t \leftarrow \text{ALG3}(\lfloor n/2 \rfloor, \min\{w, \lfloor n/2 \rfloor\}, i, S)$
 $x_{i+2\lceil n/2 \rceil} \leftarrow (0\dots, \lfloor n/2 \rfloor \text{ lowest bits of } t)$
end for
for $i = 1, \dots, 2^{\lceil n/2 \rceil} + 2^{\lfloor n/2 \rfloor} - 1$ **do**
 $y_i \leftarrow f(x_i)$
end for
 $(j_1, \dots, j_{2^{\lceil n/2 \rceil} + 2^{\lfloor n/2 \rfloor} - 1}) \leftarrow \text{SortingPermutation}(y_1, \dots, y_{2^{\lceil n/2 \rceil} + 2^{\lfloor n/2 \rfloor} - 1})$ ▷ done by sorting indices with y as key
for $i = 1, \dots, 2^{\lceil n/2 \rceil} + 2^{\lfloor n/2 \rfloor} - 2$ **do**
 if $y_{j_i} = y_{j_{i+1}}$ **then**
 return $x_{j_i} \oplus x_{j_{i+1}}$
 end if
end for
return $\{0\}^n$

ALG. 5. Building conflict graph for 2-body interactions.**Input:**
 $C = (V, E)$ — connectivity graph
Output:
 $C^{(2)}$ — conflict graph where vertices represent 2-body interactions.

```

 $C^{(2)} \leftarrow (\{1, \dots, |E|\}, \emptyset)$  ▷ Initialize conflict graph
for  $i = 1, \dots, |E| - 1$  do
  for  $j = i + 1, \dots, |E|$  do
    if  $E[i] \cap E[j] \neq \emptyset$  then
      Add edge  $(i, j)$  to  $C^{(2)}$  ▷ Interactions share a qubit
    end if
  end for
end for
return  $C^{(2)}$ 

```

Appendix A3: Detailed analysis of HUBO instances from Ref. [22]**1. HUBO instance construction**

We begin with providing a more detailed description of the HUBO instances used in Sec. IV of the main text. These instances are designed to be challenging, yet well suited for the IBM quantum computers, thus the starting point in their construction is the heavy-hex graph C_0 of IBM Heron architecture [69]. Two conflict graphs are then constructed: $C_0^{(2)}$ and $C_0^{(3)}$, with vertices corresponding to the edges of C_0 in the case of $C_0^{(2)}$, and to the triangles and three-qubit paths in the case of $C_0^{(3)}$. Edges in the conflict graphs connect vertices that share a vertex in C_0 , which means that the operations on qubits encoding these interactions cannot be executed simultaneously. By applying graph coloring to the conflict graphs, one obtains partitions of the edges of C_0 into sets of non-conflicting edges, $P_{2q} = \{P_{2q}^{(1)}, P_{2q}^{(2)}, \dots, P_{2q}^{(M_2)}\}$ and $P_{3q} = \{P_{3q}^{(1)}, P_{3q}^{(2)}, \dots, P_{3q}^{(M_3)}\}$, where M_2 and M_3 are the number of colors used in the coloring of $C_0^{(2)}$ and $C_0^{(3)}$, respectively. Each set $P_{2q}^{(i)}$ and $P_{3q}^{(i)}$ contain two- and three-body interactions that can be executed in parallel on the quantum hardware.

Interaction sets are then included in the HUBO Hamiltonian (5) by updating the G_2 and G_3 sets: $G_2 \leftarrow G_2 \cup \{P_{2q}^{(i)}\}_{i=1, \dots, S_{2q}}$ and $G_3 \leftarrow G_3 \cup \{P_{3q}^{(i)}\}_{i=1, \dots, S_{3q}}$. The parameters $S_{2q} \leq M_2$ and $S_{3q} \leq M_3$ control the number of sets of two- and three-body interactions included in the Hamiltonian, and thus directly affect the complexity of its topology. The final step is the SWAP operation, carried out using the first two-body interaction set $P_{2q}^{(1)}$, which maps $C_0 \rightarrow C_1$ by permuting all qubits pairs $(q_1, q_2) \in P_{2q}^{(1)}$. This iteration can then be repeated, successively increasing the number of interactions. After the interaction topology is prepared, the couplings are sampled from one of two distributions: (i) Cauchy, with density function $f(x) = 1/[\pi(1 + x^2)]$, and (ii) symmetrized Pareto, which starts from density function $f(x) = \alpha/x^{\alpha+1}$, but the samples are symmetrized by multiplying them by a Bernoulli distributed random sign with probability 1/2.

Like the authors of Ref. [22], we select two types of instances: (i) $S_{2q} = 1, S_{3q} = 4$, single SWAP and Cauchy distributed couplings, (ii) $S_{2q} = 1, S_{3q} = 6$, single SWAP and symmetrized Pareto distributed couplings. We also considered reduced initial couplings graphs, to obtain instances smaller than the full heavy-hex IBM Heron QPU. In the end, we generated 50 random instances per type and size $N \in [80, 100, 130, 156]$. To ensure transparency and reproducibility, we make publicly available a GitHub repository containing all generated instances together with the Python code used for their generation [62].

ALG. 6. Building conflict graph for 3-body interactions.

Input:
 $C = (V, E)$ — connectivity graph

Output:
 $C^{(3)}$ — conflict graph where vertices represent 3-body interactions.

```

 $\mathcal{I} \leftarrow \emptyset$ 
for  $v \in V$  do
   $N_v \leftarrow \{u \in V : (v, u) \in E\}$  ▷ Neighbors of  $v$ 
  for  $(u, w) \in \{(u, w) : u, w \in N_v \wedge (u, w) \in E\}$  do
     $\mathcal{I} \leftarrow \mathcal{I} \cup \{(v, u, w)\}$  ▷ All pairs of neighbors
  end for
end for
 $C \leftarrow (\{1, \dots, |\mathcal{I}|\}, \emptyset)$  ▷ Initialize conflict graph
for  $i < j \leq |\mathcal{I}|$  do
  if  $\mathcal{I}[i] \cap \mathcal{I}[j] \neq \emptyset$  then ▷ Interactions share a qubit
    Add edge  $(i, j)$  to  $C$ 
  end if
end for
return  $C$ 

```

ALG. 7. HUBO instance generation

Input:
 C_0 — starting topology graph
 S_{2q} — number of two-body interaction sets to include,
 S_{3q} — number of three-body interaction sets to include,
 n_{swap} — number of SWAP iterations,
 dist — coupling distribution

Output:
 J, K — dictionaries with two-body and three-body interactions defining the HUBO instance

```

 $G_2 \leftarrow \emptyset, G_3 \leftarrow \emptyset$ 
 $C \leftarrow C_0$ 
for  $n = 0, 1, \dots, n_{\text{swap}}$  do
   $C^{(2)} \leftarrow \text{BuildConflictGraph}(C, \text{2-body}), C^{(3)} \leftarrow \text{BuildConflictGraph}(C, \text{3-body})$ 
   $P_{2q} \leftarrow \text{GraphColoring}(C^{(2)}), P_{3q} \leftarrow \text{GraphColoring}(C^{(3)})$ 
  for  $i = 1, \dots, S_{2q}$  do
     $G_2 \leftarrow G_2 \cup P_{2q}^{(i)}$ 
  end for
  for  $i = 1, \dots, S_{3q}$  do
     $G_3 \leftarrow G_3 \cup P_{3q}^{(i)}$ 
  end for
  if  $\text{swap} < n_{\text{swap}}$  then ▷ Permute qubit pairs from first 2-body set
     $C \leftarrow \text{ApplySWAP}(C, P_{2q}^{(1)})$ 
  end if
end for
for  $(m, n) \in G_2$  do
   $J_{mn} \leftarrow \text{SampleCoupling}(\text{dist})$ 
end for
for  $(p, q, r) \in G_3$  do
   $K_{pqr} \leftarrow \text{SampleCoupling}(\text{dist})$ 
end for
return  $J, K$ 

```

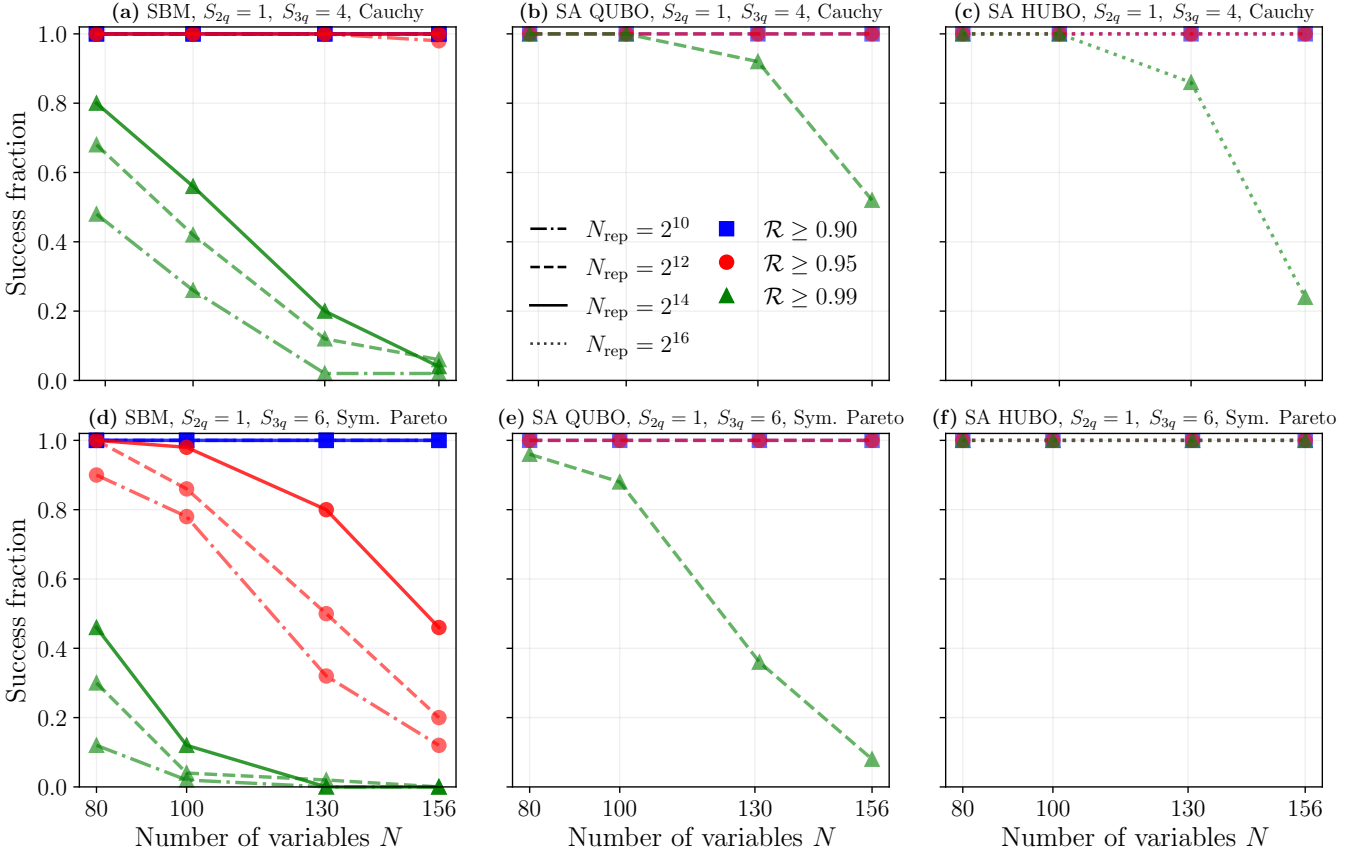


FIG. A1. Success fraction as a function of instance size, for 50 considered instances of each type. Panels (a) and (d) show results for SBM, (b) and (e) for SA in QUBO form, and (c) and (f) for SA in HUBO form. The top row (a-c) corresponds to instances with $S_{2q} = 1$, $S_{3q} = 4$, Cauchy distributed couplings, while the bottom row (d-f) to instances with $S_{2q} = 1$, $S_{3q} = 6$, symmetrized Pareto distributed couplings. These results show that, when it comes to pure solution quality, these instances are challenging for Simulated Bifurcation. However, the success fraction can be significantly improved by increasing the number of replicas evolved in parallel, for which SBM is particularly well suited. SA, both in QUBO and HUBO form, performs significantly better, with the QUBO-native version being the best for Cauchy instances, and HUBO-native for Pareto instances.

2. Performance of Simulated Bifurcation and Simulated Annealing on HUBO instances

In its usual formulation, both SBM and SA are designed to solve problems with up to second-order interactions. To apply them to HUBO instances, we first need to use some reduction technique to convert higher-order terms into quadratic ones. We choose a standard reduction method for third-order Ising interactions [70]:

$$\pm s_i s_j s_k \rightarrow 3 \pm (s_1 + s_2 + s_3 + 2s_{\text{aux}}) + 2s_{\text{aux}} (s_i + s_j + s_k) + s_i s_j + s_i s_k + s_j s_k, \quad (\text{A31})$$

which introduces one auxiliary spin s_{aux} per third-order term, and preserves the spectrum of the original problem. In the GitHub repository [62], we provide both HUBO instances and their QUBO counterparts after the reduction. We also note that SA can be extended to directly handle higher-order interactions fairly easily, and while in principle SBM can be too [71], it is much more involved. Thus, we only consider the HUBO-native version of SA, which we discuss in greater detail in App. A4.

We start by analyzing the success fraction, defined as the fraction of instances for which a given algorithm found solution better than or equal to a certain threshold. The results are shown in Fig. A1, for three selected thresholds, $\mathcal{R} \in \{0.90, 0.95, 0.99\}$, and as a function of instance size N . We see a first hint that these instances are indeed challenging, since the success fraction decreases rapidly with both instance size and the threshold approximation ratio. Interestingly, Simulated Bifurcation seems to struggle much more than Simulated Annealing, at least when it comes to pure solution quality. However, when discussing approximate optimization algorithms, one should always be mindful of the time-quality trade-off. Let us now consider the runtime of the algorithms, to see a different picture emerge. In Fig. A2, we show the approximation ratio \mathcal{R} , averaged over 50 coupling realizations and 10 (5) independent runs of SBM (SA), as a function of runtime, for each considered instance type and size. Immediately, we can notice that while

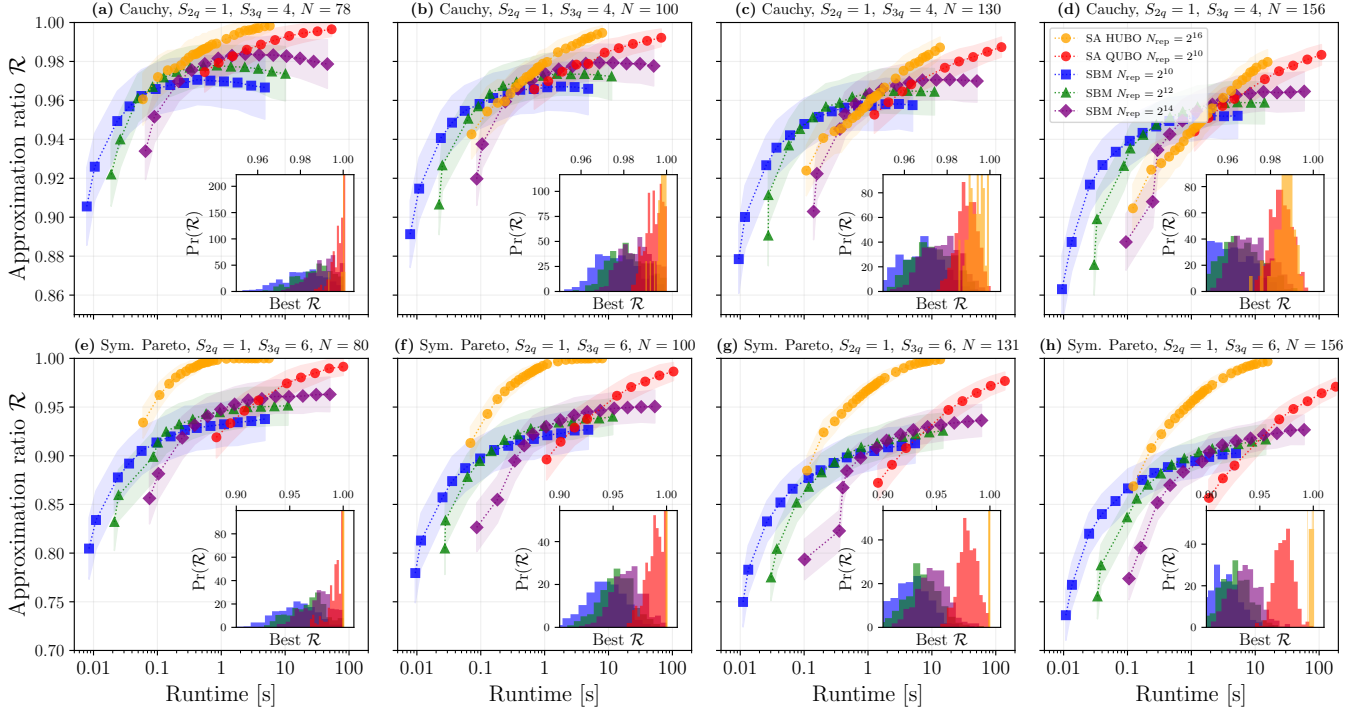


FIG. A2. Approximation ratio \mathcal{R} as a function of runtime, averaged over 50 instances and 10 (5) independent runs of SBM (SA), for each instance type and size. Shaded area corresponds to one standard deviation, and insets show the distribution of \mathcal{R} obtained, by aggregating best values for a given instance type and size. We can clearly see the biggest advantage of SBM over SA – its ability to efficiently evolve many replicas simultaneously, while keeping the runtime low. In terms of quality-runtime trade-off, it holds its ground even against the HUBO SA variant, which does not suffer overheads from rank reduction. In particular, SBM is able to, on average, reach solutions of reasonable quality, $\mathcal{R} \approx 0.95$ for Cauchy instances and $\mathcal{R} \approx 0.90$ for Pareto instances, close to an order of magnitude faster than SA, except for large Pareto instances, which seems to be “easy” for the HUBO SA. This is promising, given that it is possible to extend SBM so that it can handle higher-order interactions natively [71]. Finally, insets reveal broad distribution of approximation ratios over random coupling selection for a fixed topology, which further highlights the importance of conducting a proper statistical analysis before drawing any conclusions.

QUBO SA reaches better solutions eventually, SBM is able to reach good solutions close to an order of magnitude faster. Similar conclusions can be drawn when comparing SBM to HUBO SA in the case of Cauchy instances, while the Pareto instances seem to be “easy” for HUBO SA. Nevertheless, even in this case, the performance of SBM is still respectable, especially when considering the potential for further improvement via extending it to natively handle higher-order interactions [71].

Crucially, this is a result of a statistically sound benchmarking procedure, being aware of, and taking into account the variability of instances due to random coupling selection. The impact of selective reporting, which were discussed in the main text, here are clearly visible in the insets of Fig. A2, which show the rather broad distribution of best approximation ratios obtained for each instance type and size. To stress it again here, in Fig. A3 we reproduce Fig. 3 from the main text, but with the addition of results from an optimized, GPU-based implementation of HUBO SA. This shows that not only the choice of baseline algorithm matters, but also the specific implementation can influence the results, and one should always strive to use the best available version of a given algorithm.

Appendix A4: Simulated Annealing for QUBO and HUBO

Simulated Annealing (SA) is one of the most widely used algorithms for finding approximate solutions to combinatorial optimization problems [24]. It relies on thermal fluctuations to probabilistically escape local minima during the search process and has inspired more sophisticated variants such as parallel tempering [72], parallel annealing [73], and population annealing [74], among others [58].

In principle, SA can be applied to higher-order interactions of any order k , although it often becomes inefficient once the interaction order exceeds $k = 3$. While the method is guaranteed to converge to a local optimum, in practice convergence is limited by the chosen number of steps or runtime. As a result, the gap from the global optimum can

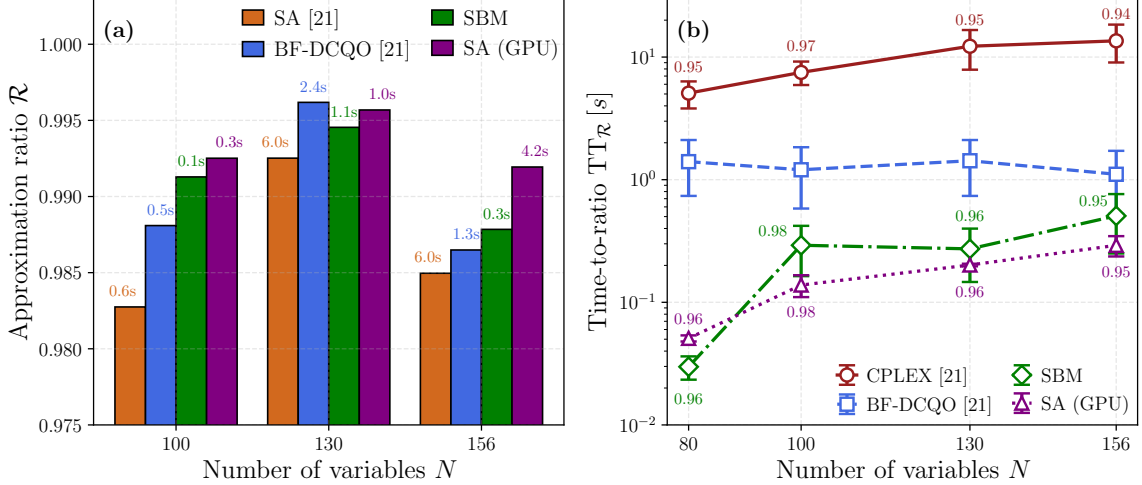


FIG. A3. Reproduction of Fig. 3 from the main text, with additional results from an optimized, GPU-based implementation of Simulated Annealing natively handling third-order interactions (cf. ALG. 9). This simulation demonstrates that an optimized HUBO SA method is already sufficient to outperform the BF-DCQO hybrid approach of Ref. [22].

remain large, especially for dense graphs [75]. Here we briefly outline the algorithm and provide pseudo-code for both QUBO and HUBO problems.

The key advantage of SA is the simplicity of its concept. It operates on a batch of trajectories, often initialized as pseudo-random spin configurations. For all the scheduled temperatures T , we perform a fixed number of passes over all variables of all trajectories. For each variable, we compute δ – the energy change that would result from flipping its value to the opposite sign. If $\delta < 0$, the flip is accepted. Otherwise, it is accepted with probability $\exp(-\delta/T)$.

The key performance aspects of SA implementation involve: parallelization strategy, data structures to store matrices, optimized recomputation of δ values. When the batch of trajectories sufficiently large, parallelizing over trajectories is effective, and avoids any potential data races, regardless of the specific approach to δ computation. While J can be stored efficiently in either dense or sparse format, the higher-order interaction tensor K is typically very sparse, including in the instances used in this paper. The proposed implementation uses CUSPARSE data structures and the `cusparseSpMM` routine for sparse-dense matrix multiplications in Alg. 9.

In the quadratic case, described as Alg. 8, δ values can be updated incrementally after each accepted flip. This makes it feasible to keep the full δ_{rv} matrix in memory – it is computed once, and updated as flips occur. For cubic problems, this optimization is not efficient, since processing slices of K involves higher dimensionality than in the case of J . For that reason, we recompute δ_r vector for each variable v . This approach guarantees that we always use δ values in sync with states as they are stored in the memory. As shown in Alg. 9, focusing on one variable at time is more efficient than updating the entire matrix at once. This mitigates the overhead of more frequent δ recomputation.

For the technical implementation purposes, we assume that 2- and 3-body interactions are presented in symmetric arrays, i.e. $J_{ij} = J_{ji}$ and $K_{ijk} = K_{jik} = K_{ikj}$ for $i, j, k \in \{1, n\}$, n being the number of variables. We also assume $J_{ii} = 0$ and $K_{iik} = 0$, since such interactions can be represented by lower-order terms. This makes it possible to rewrite the cost function from Eq. (3) as:

$$P(s) = \left(\frac{1}{6} \left(\sum_{i=1}^n (K_i s) s_i \right) + \frac{1}{2} J s + h \right)^\top s. \quad (\text{A41})$$

This formulation underlies the δ_{rv} update cost formulas presented in Alg. 8 and δ_r for Alg. 9.

Appendix A5: Reproducibility

To ensure the reproducibility of our results, we provide a GitHub repository [62]. It contains structured HUBO instances for three-body Ising models (along with generation code), a Python client for Simulated Bifurcation Machine experiments, and a CUDA-optimized Julia implementation of Simulated Annealing. The repository also includes a Python program for executing quantum circuits on IBM Brisbane, a Julia solver for Simon’s problem with various oracle configurations, and all data and scripts used to generate the paper’s figures.

ALG. 8. Simulated annealing for quadratic optimization**Input:**

$n \in \mathbb{N}$ – number of variables,
 $J \in \mathbb{R}^{n \times n}$ – symmetric matrix of 2-body interactions,
 $h \in \mathbb{R}^n$ – magnetic field,
 $m \in \mathbb{N}$ – number of trajectories (starting from initial states) to process,
 $num_steps \in \mathbb{N}$ – number of steps for consequent temperatures,
 $num_passes \in \mathbb{N}$ – number of passes over variables per temperature,
 T_0, T_1 – temperatures in the initial and the final step.

Output:

```

 $s \in \{-1, 1\}^{m \times n}$  – spectrum of near-optimal states.
 $s \leftarrow m$  pseudo-random states for  $n$ -variable problem ( $\{-1, 1\}^{m \times n}$  matrix)
 $\beta \leftarrow num\_steps$ -long geometric sequence from  $1/T_0$  to  $1/T_1$ 
 $\delta \leftarrow -2s \odot (sJ + h^\top)$   $\triangleright \delta_{rv}$  is the energy change from flipping variable  $v$  in state  $r$ 
for  $step = 1, \dots, num\_steps$  do
  for  $pass \in \{1, \dots, num\_passes\}$  do
    for  $v \in \{1, \dots, n\}$  do
      for  $r \in \{1, \dots, m\}$  do  $\triangleright$  parallelized with no need for atomic operations
        if  $\delta_{rv} < 0$  or Rand()  $< \exp(-\delta_{rv} \beta_{step})$  then  $\triangleright$  Rand yielding a pseudo-random number from (0, 1) range
           $s_{rv} \leftarrow -s_{rv}$ 
           $\delta_{rv} \leftarrow -\delta_{rv}$ 
          for  $w \in \{1, \dots, n\}$  do
             $\delta_{rw} \leftarrow \delta_{rw} - 4 J_{vw} s_{rv} s_{rw}$   $\triangleright J_{vv}$  is assumed to be 0
          end for
        end if
      end for
    end for
  end for
end for
return  $s$ 

```

Appendix A6: Hardware

All classical benchmarks in this work were performed on a workstation equipped with dual Intel(R) Xeon(R) Platinum 8462Y+ CPUs, 4 NVIDIA H100 SXM GPUs, and 1TB of RAM. All results were obtained using a single GPU, unless stated otherwise.

ALG. 9. Simulated annealing for third order HUBO optimization**Input:**

$n \in \mathbb{N}$ – number of variables,
 $K \in \mathbb{R}^{n \times n \times n}$ – tensor of 3-body interactions, symmetric under any permutation of indices,
 $J \in \mathbb{R}^{n \times n}$ – symmetric matrix of 2-body interactions,
 $h \in \mathbb{R}^n$ – magnetic field,
 $m \in \mathbb{N}$ – number of trajectories (starting from initial states) to process,
 $num_steps \in \mathbb{N}$ – number of steps for consequent temperatures,
 $num_passes \in \mathbb{N}$ – number of passes over variables per temperature,
 T_0, T_1 – temperatures in the initial and the final step.

Output:

```

 $s \in \{-1, 1\}^{m \times n}$  – spectrum of near-optimal states.  

 $s \leftarrow m$  pseudo-random states for  $n$ -variable problem ( $\{-1, 1\}^{m \times n}$  matrix)  

 $\beta \leftarrow num\_steps$ -long geometric sequence from  $1/T_0$  to  $1/T_1$   

for  $step = 1, \dots, num\_steps$  do  

  for  $pass \in \{1, \dots, num\_passes\}$  do  

    for  $v \in \{1, \dots, n\}$  do  

       $\delta \leftarrow -2(s^\top)_v \odot \left(\frac{1}{2}(sK_v \odot s) \mathbf{1}_n + s(J_v)^\top + h_v\right)$  ▷  $K_v$  –  $v$ -th matrix of  $K$ .  $(s^\top)_v$  –  $v$ -th rows  

      for  $r \in \{1, \dots, m\}$  do ▷ parallelized with no need for atomic operations  

        if  $\delta_r < 0$  or Rand()  $< \exp(-\delta_r \beta_{step})$  then ▷ Rand yielding a pseudo-random number from (0, 1) range  

           $s_{rv} \leftarrow -s_{rv}$   

        end if  

      end for  

    end for  

  end for  

end for  

return  $s$ 

```